

1 Title
2 The fungal-specific Hda2 and Hda3 proteins regulate morphological switches
3 in the human fungal pathogen *Candida albicans*.

4 Running title:

5 Hda2 and Hda3 control *C. albicans* morphogenesis

6 Misty R. Peterson^a, Robert Jordan Price^a, Sarah Gourlay^a, Alisha May^{a*}, Jennifer
7 Tullet^a and Alessia Buscaino^{a#}

8

⁹ ^a: Kent Fungal Group, School of Biosciences, University of Kent, Canterbury, United Kingdom

11

12

13 ^aAddress correspondence to Alessia Buscaino, A.Buscaino@kent.ac.uk

¹⁴ * Present address: Department of Life Sciences, Imperial College London, South
¹⁵ Kensington Campus, London, SW7 2AZ

16

17 Word Count Main Text: 3902

18 Word Count Material and Methods: 1880

19

20 **ABSTRACT**

21 The human fungal pathogen *Candida albicans* is responsible for millions of infections
22 annually. Due to the few available anti-fungal drugs and the increasing incidence of
23 drug resistance, the number of *C. albicans* infections is dramatically increasing.
24 Morphological switches, such as the white-opaque switch and the yeast-hyphae
25 switch, are key for the development of *C. albicans* pathogenic traits. Lysine
26 deacetylases are emerging as important regulators of morphological switches. Yet,
27 targeting lysine deacetylases for drug development is problematic due to the high
28 homology between the fungal and human proteins that could result in toxicity. Here
29 we provide evidence that the fungal specific proteins Hda2 and Hda3 interact with
30 the lysine deacetylase Hda1. By combining phenotypic analyses with genome-wide
31 transcriptome analyses, we demonstrate that Hda2 and Hda3 control *C. albicans*
32 morphological switches. Under nutrient-rich conditions, deletion of *HDA2* or *HDA3*
33 leads to moderate overexpression of the master regulator of white-opaque switching
34 *WOR1* and increase switching frequency. Under hyphae inducing conditions,
35 deletion of *HDA2* and *HDA3* block hyphae development. However, deletion of *HDA2*
36 and *HDA3* does not affect hyphae-formation and virulence *in vivo*. We propose that
37 Hda2 and Hda3 are good targets for the development of anti-fungal drugs to be used
38 in combination therapy.

39

40 **KEYWORDS**

41 KDACs, *Candida albicans*, morphological switches, white and opaque switch, yeast
42 to hyphae switch

43

44 INTRODUCTION

45 Fungal pathogens are a leading cause of human mortality causing over 1.5 million
46 deaths per year (1). *C. albicans* is a commensal organism that colonises the mouth,
47 gastrointestinal and reproductive tract of healthy individuals without causing any
48 harm. Still, *Candida albicans* is also the most common human fungal pathogen and
49 the principal causal agent of mycotic death (2). This is because, in immune-
50 compromised patients, *C. albicans* can invade vital organs and cause serious, life-
51 threatening systemic infections associated with a mortality rate up to 70 % (2). The
52 ability to transition between different morphological forms in response to changing
53 environments is a key virulence trait in *C. albicans*.

54 For example, *C. albicans* cells can reversibly switch between white and opaque
55 forms (3). White and opaque cells are genetically identical, yet they differ in cellular
56 morphology, colony shape, gene expression profile and mating behaviour (4). In
57 addition, white cells are more virulent in a murine model of systemic infection (5, 6)
58 whereas opaque cells preferentially colonise the skin (7). White-opaque switching is
59 under the control of the master regulator Wor1, a transcription factor whose
60 expression is necessary and sufficient for opaque cell formation (8–11). Stochastic
61 increases in Wor1 levels drives the transition from the white to the opaque phase.
62 Furthermore, Wor1 expression produces a direct positive feedback loop by binding
63 its own promoter and turning on its own expression (8, 9, 11). Switching is also
64 regulated by the mating type locus as opaque formation occurs predominantly in a or
65 α cells (12).

66 *C. albicans* virulence also depends on its ability to convert between yeast and hyphal
67 morphology: yeast cells are critical for colonisation, early infection and
68 dissemination, while hyphal growth is responsible for tissue invasion and chronic

69 infections (13). Hyphal morphogenesis is coupled with virulence, as several of the
70 genes, that are specifically expressed in hyphae, encode virulence factors (14–17).

71 Hyphal morphogenesis is a complex and highly orchestrated process, and *C.*
72 *albicans* uses multiple redundant pathways to integrate host signals and promote

73 hyphae development. Indeed, *C. albicans* filamentation can be induced by many
74 environmental cues such mammalian serum, body temperature, hypoxia and CO₂

75 concentration which reflects the variety of signals sensed by the fungus in the
76 different microenvironments encountered in the host. In yeast cells, hyphae

77 morphogenesis is inhibited by the DNA-binding repressor Nrg1 that, together with
78 Tup1, blocks expression of a subset of filament-specific genes (18). Upon hyphal

79 induction, filamentous growth is promoted by Efg1 and Flo8, two transcription
80 regulators essential for hyphal development and virulence [14–16]. During the

81 initiation phase of hyphae morphogenesis, Nrg1-mediated repression is cleared via
82 *NRG1* transcriptional repression and Nrg1 protein degradation. During hyphae

83 maintenance, chromatin remodelling of hyphae promoters prevents Nrg1 binding
84 despite its increased protein levels (19).

85 Due to the close evolutionary relationship between fungi and the human host,
86 effective treatment for *C. albicans* infections is hindered by the limited number of
87 sufficiently divergent potential drug targets. There are only three classes of
88 antifungal drugs effective for the treatment of systemic fungal infections and their
89 clinical utility is limited by the rapid emergence of drug resistance (1, 20). Hence,
90 there is an immediate and urgent need to develop alternative treatments. A potential
91 strategy is to target *C. albicans* morphological plasticity.

92 Lysine deacetylases (KDACs, also known as HDACs) act as global regulators of
93 gene expression by catalysing the removal of acetyl functional groups from the lysine

94 residues of histones and non-histone proteins (21). KDACs can favour transcriptional
95 repression by deacetylating lysine residues on histone tails allowing chromatin
96 compaction and/or preventing binding of bromodomain-containing transcriptional
97 activators (21). KDACs can also activate transcription by deacetylation of non-
98 histone proteins (22). As a consequence, deletion or inhibition of KDACs often
99 results in the upregulation and downregulation of an approximately equivalent
100 number of genes (23). KDACs are highly conserved across eukaryotes and can be
101 phylogenetically divided into three main classes: the Rpd3 and Hos2-like (class I)
102 enzymes, the Hda1-like (class II) enzymes and the Sir2-like (class III) enzymes. The
103 class I and class II enzymes are related, sharing a conserved central enzymatic
104 domain. The class III enzymes are nicotinamide adenine dinucleotide (NAD)
105 dependent. KDACs lack intrinsic DNA-binding activity and are recruited to target
106 genes via incorporation into large multiprotein complexes or direct association with
107 transcriptional activators and repressors (24).
108 In *C. albicans*, the lysine deacetylase Hda1 (class II) is an important regulator of
109 morphological switches. Hda1 controls white-opaque switching as deletion of the
110 *HDA1* gene increases switching rates from white to opaque (25, 26). In response to
111 serum, N-acetylglucosamine or nutrient limitation, Hda1 also controls the yeast to
112 hyphae switch by deacetylating Yng2, a component of the histone acetyltransferase
113 NuA4 complex, blocking maintenance of hyphal growth (19). However, the Hda1
114 pathway is not required for hyphae elongation in hypoxia or in the presence of
115 elevated CO₂ because of the presence of redundant pathways (27, 28). As a result,
116 the Hda1-mediated hyphae maintenance pathway contributes, but it is not absolutely
117 required, for virulence *in vivo* (27). These results suggest that Hda1 is a good target
118 for antifungal drugs development to be used in combination therapies.

119 KDACs are promising druggable targets: one KDAC inhibitor is currently used for
120 cancer treatment and several other KDAC inhibitors are in clinical trials (29, 30).
121 However effective targeting of Hda1 for anti-fungal drug development is impaired by
122 the high sequence similarities between Hda1 and its human orthologs and
123 consequently a likeliness for high toxicity.

124 In *Saccharomyces cerevisiae*, Hda1 assembles with two non-catalytic subunits,
125 Hda2 and Hda3, essential for Hda1 deacetylation activity both *in vivo* and *in vitro*
126 (31). Interestingly, no metazoan homologous of Hda2 and Hda3 have been
127 identified. Hda2 and Hda3 are similar in sequence and share a similar protein
128 organisation with an N-terminal DNA binding domain (DBD) and a C-terminal coil-coil
129 domain (CCD). The DBD domain, similar in structure to the helicase domain of the
130 SWI-SNF chromatin remodelers, is sufficient to bind DNA *in vitro*. The CCD domains
131 act as a scaffold for the assembly of the Hda1 complex (32).

132 Here for the first time, we analyse the role of *C. albicans* Hda2 and Hda3. We
133 demonstrate that the Hda1 complex is conserved in *C. albicans* as Hda2 and Hda3
134 interact with Hda1 *in vivo*. Our analyses demonstrated that, in yeast-inducing
135 conditions, deletion of *HDA2* and *HDA3* leads to transcriptional upregulation of
136 *WOR1* and that Hda2 and Hda3 inhibit white and opaque switching. In contrast,
137 under hyphae-inducing conditions, Hda2 and Hda3 regulate the yeast to hyphae
138 switch. This functional rewiring is linked to a reduced expression of components of
139 the Hda1 complex. Our study demonstrates that Hda2 and Hda3 control key
140 morphological switches in *C. albicans*. Therefore, we propose that Hda2 and Hda3
141 are attractive targets for the development of novel antifungal drugs.

142 **RESULTS**

143 **The Hda1 complex is conserved in *C. albicans***

144 *S. cerevisiae* Hda2 and Hda3 are critical components of the Hda1 complex as they
145 are required for the Hda1-mediated histone deacetylation activity (31). BLAST
146 analyses reveal that the *C. albicans* genome contains two genes encoding proteins
147 with homology to *S. cerevisiae* Hda2 (C3_03670W) and Hda3 (CR_09490W_A).
148 Structural alignments predict that Hda2 and Hda3 have a similar protein organisation
149 with an N-terminal DNA binding domain (DBD) and a C-terminal coil-coil domain
150 (CCD) (Fig 1A and 1B). To explore the potential functional relationship between *C.*
151 *albicans* Hda2, Hda3 and Hda1, we assessed whether we could detect a physical
152 interaction between these proteins. To this end, we generated strains expressing at
153 the endogenous locus an epitope-tagged Hda1 protein (Hda1-HA) together with
154 either Hda2-GFP or Hda3-GFP. Western analyses show that the Hda1-HA and
155 Hda2-GFP tagged proteins are expressed at high levels while we could not detect
156 Hda3-GFP in whole cell extract indicating that the protein is expressed at low levels
157 (Fig 1C). Immuno-precipitation (Ip) of Hda1-HA with a highly specific anti-HA
158 antibody demonstrates that Hda2 strongly interacts with Hda1. We could also detect
159 an interaction between Hda1 and Hda3, despite the low level of expression of Hda3
160 (Fig 1C). Thus, Hda2 and Hda3 physically interact with Hda1. To delineate the
161 function of *C. albicans* Hda2 and Hda3, we generated homozygous deletions
162 mutants for *HDA2* (*hda2* Δ/Δ) and *HDA3* (*hda3* Δ/Δ) genes using a recyclable Clox
163 system (Fig 1D) (33). The Clox system allows for the generation of a homozygous
164 deletion mutant lacking any marker genes and therefore genetically identical to the
165 parental strain except for the deleted gene. This allows for the direct comparison of
166 phenotypes between mutant and parental strains. Growth analyses reveal that Hda2
167 and Hda3 are not required for survival and fitness as the *hda2* Δ/Δ and *hda3* Δ/Δ

168 strains grow similarly to the wild-type (WT) control both on solid and in liquid media
169 (Fig 1E and 1F). Therefore, *C. albicans* Hda2 and Hda3 are *bona fide* components of
170 the Hda1 complex that are not required for cell fitness and survival under optimal
171 growth conditions.

172

173 **Global gene expression changes in the absence of Hda2 and Hda3**

174 To gain insights about the function of Hda2 and Hda3 in conditions stimulating yeast
175 growth, we analysed changes in gene expression by strand-specific RNA-
176 sequencing (RNA-seq) upon deletion of the *HDA2* and *HDA3* genes. As a
177 comparison, we also performed RNA-seq on strains with the *HDA1* gene deleted.
178 Deletion of *HDA2* results in 577 genes significantly differentially regulated (348
179 upregulated and 229 downregulated, $q < 0.05$; Dataset S1). These gene expression
180 changes are highly similar to the ones observed in *hda1* Δ/Δ (Pearson correlation
181 coefficient $r = 0.7$, Dataset S1) (Fig 2A). Deletion of the *HDA3* gene has a less
182 profound effect on gene expression as only 78 genes are significantly differentially
183 expressed (45 upregulated and 33 downregulated, $q < 0.05$; Dataset S1). Despite
184 this difference, changes in *hda3* Δ/Δ cells correlate with *hda1* Δ/Δ and *hda2* Δ/Δ gene
185 expression changes (Pearson correlation coefficient $r = 0.66$ and 0.46 , respectively)
186 (Fig 2A).

187 To reveal the cellular pathways regulated by Hda2 and Hda3 in *C. albicans*, we
188 performed Gene Set Enrichment Analysis (GSEA) of the RNA-seq datasets (34). To
189 this end, transcript profiles of *hda2* Δ/Δ or *hda3* Δ/Δ isolates were ranked according
190 to their differential expression and this list was compared to gene sets identified in
191 other experimental analyses (35) and (Sellam et al, personal communications). This

192 allows the identification of statistically significant gene sets enriched in the top (up-
193 regulated) or the bottom (down-regulated genes) of the ranked list (34). The network
194 of similar gene sets was visualized using Cytoscape where nodes represent gene
195 sets, and lines connect nodes sharing a significant number of genes (36).

196 GSEA detected enrichment for rRNA and ribosome biogenesis genes and genes
197 involved in transport (Fig 2B). Enrichment was also found in gene sets important for
198 virulence-promoting function in *C. albicans*. This includes genes differentially
199 expressed during *C. albicans*-host interactions with mouse macrophages and in
200 response to drugs (Fig 2C).

201 Modulation of several gene sets enriched in *hda2* Δ/Δ and/or *hda3* Δ/Δ mutants, for
202 example, down-regulation of genes required for protein synthesis, are part of stress
203 response in *C. albicans* (37). Accordingly, we subjected the *hda2* Δ/Δ and *hda3* Δ/Δ
204 mutants to a phenotypic analysis by applying a set of different stress conditions (38).

205 For most conditions, we did not observe any difference between the WT and the
206 mutant strains. However, lack of Hda2 or Hda3 leads to sensitivity to copper, sodium
207 chloride and sodium nitroprusside (SNP) with salicylhydroxamic acid (SHAM).
208 Strains mutant in these proteins also show resistance to rapamycin (Fig 3) indicating
209 a role for Hda2 and Hda3 in specific stress responses.

210

211 **Hda2 and Hda3 inhibit white-opaque switching**

212 The GSEA analysis identifies white-opaque switching as a process potentially
213 regulated by Hda2 and Hda3 as genes upregulated in the opaque state are also
214 upregulated upon deletion of *HDA2* and *HDA3* (Fig 4A and 4B). Wor1 is the master
215 regulator of white-opaque phenotypic switching and a stochastic increase in Wor1
216 levels drives the transition from the white to the opaque phase (8, 9, 11). Therefore,

217 we asked whether *WOR1* expression levels were increased in *hda2* Δ/Δ and *hda3*
218 Δ/Δ isolates compared to WT cells.

219 The RNA sequencing analysis demonstrates that deletion of *HDA2* or *HDA3* leads to
220 transcriptional upregulation of *WOR1* (Fig 4C). This result suggests that, in WT cells,
221 Hda2 and Hda3 repress *WOR1* transcription and inhibit white-opaque switching. To
222 test this hypothesis, we generated *MTL a/a* homozygous *hda2* Δ/Δ and *hda3* Δ/Δ
223 mutants and measured the frequency of white to opaque conversion using
224 quantitative switching assays. Briefly, cells were plated on Phloxine B plates and the
225 frequency of opaque colonies or colonies containing at least one opaque sector was
226 scored. This analysis demonstrates that deletion of both *HDA2* and *HDA3* increases
227 the frequency of white-opaque switching (Fig 4D). Thus, Hda2 and Hda3 control
228 white-opaque switching, a process that is linked to *WOR1* overexpression.

229 **Hda2 and Hda3 contribute to filamentous growth but not virulence**

230 To investigate the role of Hda2 and Hda3 under hyphae-inducing conditions, we
231 performed RNA-seq analyses of WT, *hda2* Δ/Δ and *hda3* Δ/Δ strains grown in RPMI,
232 a medium which mimics human physiological conditions and therefore strongly
233 induces hyphal growth. As a control, RNA-seq analyses were also performed in *hda1*
234 Δ/Δ strain. GSEA analysis of the gene expression changes of WT cells grown in
235 yeast-inducing conditions (YPD) and hyphae-inducing conditions (RPMI) confirmed
236 the validity of our experimental approach as genes reported to be upregulated in
237 hyphae compared to yeast are less expressed in YPD compared to RPMI while
238 genes with a yeast-specific expression are expressed at higher levels in YPD than
239 RPMI (Fig 5A).

240 In hyphae-inducing conditions, deletions of *HDA2* and *HDA3* genes result in 350 and
241 484 significantly differentially expressed genes, respectively ($q < 0.05$; Dataset S1).
242 Gene expression changes in *hda2* Δ/Δ and *hda3* Δ/Δ correlate with gene expression
243 changes observed in *hda1* Δ/Δ although less profoundly than in yeast-inducing
244 conditions (Pearson correlation coefficient, $r = 0.55$ and 0.38 , respectively; Fig 5B).
245 The RNA-seq analysis reveals that filamentation is the major pathway misexpressed
246 in the deletion mutants as hyphae-responsive genes are differentially expressed in
247 *hda2* Δ/Δ and *hda3* Δ/Δ isolates compared to WT cells (Fig 5C). qRT-PCR analyses
248 of two hyphal growth markers, *HWP1* and *ALS3*, confirmed the RNA-seq results as,
249 in hyphae inducing conditions, expression of *HWP1* and *ALS3* is downregulated in
250 *hda2* Δ/Δ and *hda3* Δ/Δ but not in WT cells (Fig 5D).
251 Collectively, our results suggest that Hda2 and Hda3 are important for hyphal
252 growth. To test this hypothesis, we assessed the morphology of WT, *hda2* Δ/Δ and
253 *hda3* Δ/Δ strains upon growth in two different hyphae-inducing media (RPMI and
254 Spider). While WT cells form hyphae efficiently, hyphal growth is defective in *hda2*
255 Δ/Δ and *hda3* Δ/Δ cells on both solid and in liquid media (Fig 6A and B). This
256 phenotype was rescued by reintroduction of the *HDA3* gene (Fig 6C). Therefore,
257 Hda2 and Hda3 are important regulators of the yeast to hyphae switch.
258 To test whether the hyphae-defective phenotype observed in *hda2* Δ/Δ and *hda3* Δ/Δ
259 isolates is sufficient to impair hyphal growth *in vivo*, we performed killing assays
260 using the nematode *Caenorhabditis elegans* as an infection system (39, 40). These
261 analyses revealed no differences in hyphae formation or percentage of killing
262 between WT, *hda2* Δ/Δ and *hda3* Δ/Δ strains (Fig 6D). Therefore, although Hda2 and
263 Hda3 are critical for hyphae-formation in specific media, additional redundant

264 pathways can compensate for the lack of Hda2 and Hda3 in a more complex *in vivo*
265 situation.

266 **Stability of Hda1 protein is regulated by environmental changes**

267 Comparison of the gene expression profiles in yeast-promoting conditions (YPD 30
268 °C) and hyphae-promoting conditions (RPMI 37 °C) reveals that deletion of *HDA1*
269 leads to different transcriptional changes in different environments (Fig 7A). In yeast
270 inducing conditions, 2046 genes are significantly differentially expressed upon
271 deletion of Hda1 compared to WT cells, suggesting that Hda1 acts as a global
272 regulator of gene expression (Fig 7A and Dataset S1). In contrast, in hyphae
273 inducing conditions, 507 genes are significantly differentially expressed with hyphal
274 growth being one of the major pathways that is altered (Fig 7B and Dataset S1).
275 These results suggest that Hda1 function is rewired during the yeast to hyphae
276 switch. We hypothesise that this change in function could be due to a differential
277 gene expression profile of *HDA1* in yeast compared to hyphae. While analysis of the
278 RNA-seq dataset reveals that *HDA1*, *HDA2* and *HDA3* transcription levels are similar
279 across these two conditions, Western analyses clearly demonstrate that levels of
280 Hda1 and Hda3 proteins, but not Hda2, are lower in hyphal cells compared to yeast
281 cells (Fig 7C). Therefore, the functional rewiring of the Hda1 complex upon an
282 environmental change is linked to a reduced expression of this subunit.

283 **DISCUSSION**

284 **The role of the Hda1 complex in regulating morphological switches in *C.***
285 ***albicans***

286 Results presented in this study show that the fungal-specific proteins Hda2 and
287 Hda3 are important regulators of morphological switches in *C. albicans*. We propose

288 that this regulation is mediated via the Hda1 complex. This hypothesis is supported
289 by our observation that Hda1, Hda2 and Hda3 physically interact and by the
290 published results demonstrating that Hda1 controls both the white-opaque and the
291 yeast-hyphae morphological switches (19, 25, 26). Based on the data presented
292 here, it is possible that Hda2 and Hda3 control the activity of the Hda1 complex by
293 different non-mutually exclusive mechanisms. First, Hda2 and Hda3 could mediate
294 Hda1 recruitment to target sites regulating their chromatin acetylation state and their
295 transcriptional activity. Indeed, in *S. cerevisiae*, Hda2 and Hda3 DNA-binding
296 domains are sufficient to bind DNA *in vitro* (32). The structural alignment presented
297 in this study demonstrates that, similar to *S. cerevisiae*, *C. albicans* Hda2 and Hda3
298 contain a DNA binding domains with structure resembling the helicase fold found in
299 the SWI2/SNF2-type chromatin-remodeling ATPase (32). We hypothesise that Hda2
300 and Hda3 could target Hda1 to key genomic locations leading to transcriptional
301 downregulation of associated genes. In support of this hypothesis, we have found
302 that *WOR1*, the master regulator of white-opaque switching, is moderately
303 upregulated in cells deleted for *HDA2* and *HDA3* genes. A similar upregulation is
304 observed in *hda1* Δ/Δ isolates. We propose that this upregulation is sufficient to
305 activate the Wor1 positive feedback loop promoting white-opaque switching. Indeed,
306 *hda2* Δ/Δ and *hda3* Δ/Δ cells undergo white-opaque switching more frequently than
307 WT cells.

308 Alternatively, interactions between Hda1, Hda2 and Hda3 may induce a
309 conformational change promoting Hda1 deacetylase activity. In support of this
310 hypothesis, it has been established that the *in vitro* catalytic activity of *S. cerevisiae*
311 Hda1 depends on Hda2 and Hda3 (31). This regulation could be critical for
312 controlling deacetylation of non-histone substrates. For example, *C. albicans* Hda1

313 controls the yeast to hyphae switch by deacetylating a non-histone substrate, the
314 NuA4 component Yng2 (19). We hypothesise that interaction between Hda1, Hda2
315 and Hda3 causes a conformational change in Hda1 allowing deacetylation of Yng2.
316 Chromatin modifiers are ideal sensors of changing environments as they can
317 respond to external stimuli by rapidly and reversibly changing the transcriptional
318 state of many genes simultaneously. Our results indicate that the activity of the Hda1
319 complex is rewired in different environmental conditions. While in yeast cells, Hda1
320 acts as a globular regulator of gene expression, in hyphae-inducing conditions Hda1
321 function is dedicated to the yeast-hyphae switch. This functional rewiring is
322 accompanied by changes in the protein levels of Hda1 and Hda3. These findings
323 suggest a model through which hyphae-specific function is achieved by diminishing
324 the concentration of key proteins of the Hda1 complex. We did not observe any
325 changes in the RNA levels of *HDA1* and *HDA3* and therefore we hypothesise that
326 translation efficiency and/or stability of these two proteins is differentially regulated in
327 different environments.

328 Chromatin modifiers are often embedded in multiprotein complexes associated with
329 several non-catalytic subunits that regulate their targeting to substrates or their
330 catalytic activity (24). Our results highlight how Hda2 and Hda3, the non-catalytic
331 subunits of the Hda1 complex, play important roles in regulating morphological
332 switches in response to environmental changes.

333 **Hda2 and Hda3 as potential targets for anti-fungal therapy**

334 The yeast to hyphae switch is central to *C. albicans* virulence and pathogenesis. Our
335 results signify that while Hda2 and Hda3 promote hyphae formation under specific
336 growth conditions (RPMI and Spider media at 37 °C), they are dispensable for
337 hyphae formation and virulence in the *C. elegans* infection system. We hypothesise

338 that this is due to the presence of redundant pathways that stimulate hyphae
339 formation. Indeed, it has been shown that hyphae induction is a highly orchestrated
340 process integrating several different environmental signals (13). The finding that, *in*
341 *vivo*, lack of Hda2 and Hda3 does not impair hyphae formation is in agreement with
342 the observation that strains mutant for the YNG2 gene, the target of Hda1, also do
343 not impair hyphae growth *in vivo* while they are defective for hyphae formation *in*
344 *vitro* (27).

345 There is an urgent need to develop new anti-fungal drugs due to emergence of
346 fungal strains resistant to currently available drugs. We propose that Hda2 and Hda3
347 could be targets for novel antifungal drugs to be used in combination therapy.

348 Combination therapy offers several advantages compared to single-drug therapy.

349 This is because it allows for widening of the spectrum and potency of drug activity
350 and it can also lead to reduction in the dosage of individual agents preventing
351 emergence of antifungal resistance (41). Several features make Hda2 and Hda3
352 attractive targets for antifungal drug development. First and most importantly, the
353 proteins are present in fungi but absent in humans minimising potential toxicity.

354 Secondly, drugs targeting Hda2 and Hda3 could have a broad spectrum of activity
355 against a variety of human fungal pathogens as Hda2 and Hda3 orthologs are
356 present in other human fungal pathogens, such as *C. glabrata* (CAGL0H01331g and
357 CAGL0G09867g) and *A. fumigatus* (Hda2: Afu5g03390).

358 KDACs are emerging as promising candidates for drug development and several
359 small molecules inhibiting KDAC activity are currently in clinical trials as potential
360 anti-cancer therapeutics. We propose that inhibition of Hda2 and Hda3 will impair *C.*
361 *albicans* Hda1 activity but not human KDACs reducing the risk of toxicity.

362 **MATERIAL AND METHODS**

363 **Growth conditions**

364 Strains are listed in Table 1. Yeast cells were cultured in rich medium (YPD)
365 containing extra adenine (0.1 mg/ml) and extra uridine (0.08 mg/ml), complete SC
366 medium (Formedium) or RPMI medium (Sigma-Aldrich). When indicated, media
367 were supplemented with 30 µg/ml doxycycline. For analysis in stress conditions,
368 YPD agar media was supplemented with 9 nM rapamycin, 2 M sodium chloride, 1
369 mM SNP with 1 mM SHAM, 7 mM copper sulphate, 300 mM lithium chloride, .01 %
370 sodium dodecyl sulfate (SDS), 15mM caffeine, 1.5 M sorbitol, 18 mM cycloheximide,
371 1.5 mM cobalt, 25 mM hydroxyurea, 3 % ethanol, 20 µM Calcofluor White, 4.5 mM
372 hydrogen peroxide, 0.75 mM EDTA and 2 µM Cerulenin (42). Cells were grown at 30
373 °C or 37 °C as indicated.

374 **Plasmid construction**

375 Oligos and plasmids used in this study are listed in Table 2 and 3. Plasmid ABp133
376 contains the *C. albicans* *HDA1* gene cloned in frame to a C-terminal HA tag. To
377 generate this plasmid, the full length *HDA1* gene was amplified from plasmid ABp88
378 (synthesised by GeneArt) with oligos Abo408 and Abo409, containing recognition
379 sites for *Xma*I. The digested PCR product was cloned into plasmid pHA-NAT
380 (ABp17)(43) digested with *Xma*I. Cloning was confirmed by PCR and Sanger
381 sequencing. *HDA3* was cloned in the pNIM plasmid (ABp111) (44) to generate
382 plasmid ABp177. For this purpose, the full length *HDA3* gene was amplified from
383 plasmid ABp152 (synthesised by GeneArt) with oligos ABo624 and ABo625,
384 containing *Xho*I and *Bgl*II restriction sites. ABo625 also supplied a stop codon
385 upstream the restriction site. This PCR fragment was cloned in pNIM digested with
386 *Sal*I and *Bgl*II. Cloning was confirmed by PCR and Sanger sequencing.

387 **Construction of *C. albicans* mutants**

388 Deletions of *HDA2* and *HDA3* were generated in the SN152 or BWP17 background
389 using the *Clox* system for gene disruption (33) using long-oligos PCR, the LAL (loxP-
390 ARG4-loxP) and NAT1-Clox (loxP-NAT1-MET3p-cre-loxP) plasmids as templates.
391 During all selections for *Clox* transformants media was supplemented with 2.5 mM
392 methionine and 2.5 mM cysteine to repress the *MET3* promoter and minimize Cre-
393 /loxP mediated recombination. Nourseothricin resistant (Nou^R) transformants were
394 selected using 200 µg/ml nourseothricin (Melford). *HDA2* and *HDA3* gene deletions
395 were confirmed by PCR and markers were resolved by allowing Cre expression in
396 medium lacking methionine and cysteine as previously described (33).
397 C-terminal GFP tagging of *HDA2* and *HDA3* genes at the endogenous loci was
398 performed by long oligos PCR using plasmid pGFP-His1 (ABp11) as a template (45).
399 C-terminal HA tagging of *Hda1* was performed by long oligos PCR using plasmid
400 ABp133 as a template and transformation into BWP17 (ABy215), HDA2-GFP
401 (ABy532) and HDA3-GFP (ABy376).
402 For rescue experiments, *HDA3* re-integrated at the *ADH* locus by digesting ABp177
403 with *Kpn*I and *Sac*II and transforming the product into the *hda3* Δ/Δ (ABy33) deletion
404 strain. Correct integration was confirmed by colony PCR. Transformations of *C.*
405 *albicans* strains were performed by electroporation using the protocol described in
406 (46) or by lithium acetate transformation (47) of competent cells (48) with a *S.*
407 *cerevisiae* method adapted to *C. albicans* (49).

408 **Hyphal growth induction and quantification**

409 Cultures were grown overnight (~16 hours) in 5 ml liquid YPD at 30 °C. Overnight
410 cultures were diluted 1:100 in YPD media and grown ~5 hours at 30 °C. 50 – 100
411 cells were plated to RPMI or Spider agar and incubated for ~6 days at 37 °C. For
412 doxycycline induction, the drug was added to the media at 30 µg/ml in 20 ml plates.

413 Phenotypes were documented by imaging with a Leica MZFLIII microscope at 10x to
414 16x magnification. A minimum of 150 colonies were counted for each strain. For
415 liquid filamentation assays, overnight cultures were grown throughout the day and
416 from this stationary culture, 1 mL was harvested and washed with distilled water
417 before resuspending in 10 mL pre-warmed final media (YPD (control) or RPMI).
418 These cultures were grown at 37 °C (control at 30 °C) for 15-17 hours before
419 imaging on an Olympus IX81 inverted microscope at 60x magnification. Samples
420 were evaluated on four separate days and a minimum of 400 cells were counted per
421 sample.

422 **White-opaque switching essay**

423 Quantitative switching assays were performed as previously described (12) with
424 modifications. Briefly, strains were streaked from frozen stocks on YPD plates and
425 grown at 30 °C for 2 days. Single colonies were picked, resuspended in sterile water
426 and spread onto synthetic complete agar containing 5 µg/ml Phloxine B (Sigma-
427 Aldrich). Formation of opaque colonies or sectors was scored after 9 days.
428 Experiments were done in biological duplicate or triplicate on at least three separate
429 days. A minimum of 400 total colonies were counted for each strain.
430 The ggplot package in R studio was used to construct violin plots. Unpaired t-tests
431 were performed to test for significant differences between wild-type and mutant
432 strains.

433 **Structural modelling**

434 The model of Hda3 DBD and CCS domain was produced using Phyre2 in intensive
435 mode (50) and visualised using PyMol (The PyMOL Molecular Graphics System,
436 Version 1.8 Schrödinger, LLC.)

437 **Whole cell extracts**

438 Preparation of whole cell extracts was performed as described (51). Briefly,
439 overnight YPD cultures were diluted in YPD or RPMI and grown to $OD_{600} = \sim 0.8$ at
440 30 °C. Cells were harvested, resuspended in 200 μ l lysis buffer (0.1 M NaOH, 0.05
441 M EDTA, 2 % SDS, 2% β -mercaptoethanol) and heated for 10 minutes at 95 °C
442 before adding 5 μ l of 4 M Acetic acid and incubating for further 10 minutes at 90 °C.
443 Extracts were mixed with 50 μ l loading buffer (0.25 M Tris-HCl pH 6.8, 50 %
444 Glycerol, 0.05 % Bromophenol Blue), incubated at 96 °C for 5 minutes and
445 centrifuged at 13000 rpm for 5 minutes. Supernatants were collected and analysed
446 by SDS-PAGE and Western blot analyses.

447 **Immunoprecipitation**

448 Immunoprecipitation was performed as described (52) with modifications. 1 L YPD
449 cultures ($OD_{600} = 1$) were harvested at 4000 rpm. Cell were washed 3 times in cold
450 water and resuspended in 1/5th volume (water/cells). Cell pellets were ground in
451 liquid nitrogen using a mortar and pestle for 30 minutes and resuspended in 10 ml of
452 cold lysis buffer (50 mM HEPES-NaOH pH 7.5, 150 mM NaCl, 5 mM EDTA, 0.1 %
453 NP-40, 5 mM DTT, 1x Roche EDTA-free protease inhibitor cocktail and 0.2 mM
454 PMSF added fresh before use). The cells were solubilized for 30 minutes with
455 rotation at 4 °C. Following centrifugation, supernatant samples were incubated with 4
456 μ l of magnetic beads pre-coupled with anti-HA antibody (Sigma-Aldrich) for 2 hours
457 with rotation at 4 °C. Beads were washed four times in lysis buffer and analysed by
458 SDS-PAGE and Western blot.

459 **Antibodies information**

460 The following antibodies were used for Western analyses. Anti-HA antibody
461 (#11666606001, Sigma-Aldrich) diluted at 1:1000, anti-GFP antibody (Roche

462 #1184460001) diluted at 1:5000, anti-actin (Cooper Lab, Washington University, St.
463 Louis, Mo., USA) diluted at 1:5000.

464 **RNA extraction**

465 Overnight YPD cultures were diluted in YPD and grown to OD₆₀₀ = ~0.8. Cells were
466 pelleted, washed once with sterile water and resuspended in pre-warmed YPD (30
467 °C) or RPMI (37 °C) for 90 minutes. RNA extraction was performed using a yeast
468 RNA extraction kit (E.Z.N.A. Isolation Kit RNA Yeast, Omega Bio-Tek) following
469 the manufacturer's instructions with the following modifications: (1) 30 °C
470 incubation in SE Buffer/2-mercaptoethanol/lyticase solution time was increased to 90
471 minutes; (2) lysis was performed with bead mill at top speed for 30 minutes at 4°C.
472 RNA was treated with DNase I and RNA quality was checked by electrophoresis
473 under denaturing conditions in 1% agarose, 1x HEPES, 6% Formaldehyde
474 (Sigma-Aldrich). RNA concentration was measured using a NanoDrop ND-1000
475 Spectrophotometer. cDNA synthesis was performed using qPCRBIo cDNA
476 Synthesis Kit (PCR Biosystems) following manufacturer's instructions.

477 **High-throughput RNA sequencing**

478 Strand-specific cDNA Illumina Barcoded Libraries were generated from 1 µg of
479 total RNA extracted from WT, *hda1* Δ/Δ, *hda2* Δ/Δ and *hda3* Δ/Δ and sequenced
480 with an Illumina iSeq2000 platform. Illumina library preparation and deep-
481 sequencing was performed by the Genomics Core Facility at EMBL (Heidelberg,
482 Germany). RNA sequencing was performed in duplicates. Raw reads were
483 analysed following the RNA deep sequencing analysis pipeline using the Galaxy
484 platform (<https://usegalaxy.org/>). Downstream analysis of differential expressed
485 genes was performed with R Studio (<https://www.rstudio.com/>). Scatter Plot
486 matrices, using Pearson correlation coefficients, were generated with the ggplot

487 package. Heatmaps were generated with the pheatmap package and Pearson
488 correlation for clustering. Heatmaps show the log2 fold changes of differentially
489 expressed genes in *hda1* Δ/Δ, *hda2* Δ/Δ or *hda3* Δ/Δ compared to wild-type
490 expression. Venn diagrams were generated using the FunRich programme(53).
491 RNA sequencing data are deposited into ArrayExpress (accession number: E-
492 MTAB-6920).

493 **qRT-PCR**

494 qRT-PCR was performed in the presence of SYBR Green (Bio-Rad) on a Bio-Rad
495 CFXConnect Real-Time System. Data was analysed with Bio-Rad CFX Manager 3.1
496 software and Microsoft Excel. Enrichment was calculated over actin. Histograms
497 represent data from three biological replicates. Error bars: standard deviation of
498 three biological replicates generated from 3 independent cultures of the same strain.

499 **Functional analysis and modelling of transcriptional profiles**

500 Gene set enrichment analysis (GSEA) (34, 54) was performed using the GSEA
501 PreRanked tool to determine whether a ranked gene list exhibited statistically
502 significant bias in their distribution within defined gene sets (55) and (Sellam *et al*,
503 personal communication). The weighted enrichment statistics were calculated on
504 10512 gene sets each containing 5-1000 genes, and the false discovery rate (FDR)
505 was calculated from 1000 permutations. Selected results graphs are shown. Since
506 enrichment profiles can exhibit correlations with hundreds of overlapping gene sets,
507 Cytoscape 3.6 (<http://www.cytoscape.org>) (56) and the Enrichment Map Pipeline
508 Collection plug-ins (<http://apps.cytoscape.org/apps/enrichmentmappipelinecollection>)
509 were used to further organise and visualise the GSEA. Enrichment maps were
510 calculated using default parameters.

511 ***C. albicans*-*C. elegans* pathogenesis assay**

512 The *C. elegans* *glp-4/sek-1* strain was used as described previously (39, 57). Briefly,
513 *C. elegans* were propagated on nematode growth medium (NGM) on lawns of *E. coli*
514 OP50. The *C. albicans*-*C. elegans* pathogenesis assay was performed as previously
515 described (40). Briefly, 100 μ l of *C. albicans* cells from an overnight culture were
516 spread into a square lawn on a 10 cm plate containing brain-heart infusion (BHI)
517 agar and kanamycin (45 μ g/ml). These were incubated for approximately 20 hours at
518 30 °C. Synchronized adult *C. elegans* *glp-4/sek-1* nematodes grown at 25°C were
519 carefully washed from NGM plates using sterile M9 buffer. Approximately 100 to 200
520 washed animals were then added to the centre of the *C. albicans* lawns and the
521 plates were incubated at 25°C for 4 hours. Worms were then carefully washed into a
522 15 ml tube using 10 ml of sterile M9, taking care to minimize the transfer of yeast.
523 Worms were washed four or five times with sterile M9. 30-40 worms were then
524 transferred into three wells of a six-well tissue culture plate (Corning, Inc.) containing
525 2 ml of liquid medium (80% M9, 20% BHI) and kanamycin (45 μ g/ml). Worms were
526 scored daily into one of three categories: alive, dead with hyphae piercing the cuticle,
527 and dead without hyphae piercing the cuticle. Worms were considered to be dead if
528 they did not move in response to mechanical stimulation with a pick. Dead worms
529 were removed from the assay. *C. elegans* survival was examined by using the
530 Kaplan-Meier method and differences were determined by using the log-rank test
531 using OASIS 2 tool (58). Differences in the number of worms with *C. albicans* hyphal
532 formation were determined by using a one-way ANOVA with Dunnett's test for
533 multiple comparisons. The *C. elegans* pathogenesis assay presented here is an
534 average of three independent biologic replicates. A p-value of <0.05 was considered
535 statistically significant.

536 **FUNDING INFORMATION**

537 A.B and R.J.P: Medical Research Council [MR/M019713/1]; S.G: [BB/L008041/1].

538 Funding for open access charge: University of Kent.

539 **ACKNOWLEDGMENTS**

540 We thank GeneCore at EMBL for performing Illumina library preparation and
541 sequencing. We thank Dr Sellam (Biotechnology Research Institute, National
542 Research Council of Canada) and Dr Traven (Monash University) for help with the
543 GSEA analysis. We are grateful to Dr Anderson (The Ohio State University) for the
544 plasmid allowing deletion of mating type cassette and Prod Alistair Brown (University
545 of Aberdeen) for the Clox system. We thank members of the Kent Fungal Group for
546 useful discussions and critical reading of the manuscript.

547

548 **REFERENCES**

549 1. Brown GD, Denning DW, Gow NAR, Levitz SM, Netea MG, White TC. 2012.
550 Hidden Killers: Human Fungal Infections. *Sci Transl Med* 4:165rv13-165rv13.

551 2. Pfaller MA, Diekema DJ. 2010. Epidemiology of invasive mycoses in North
552 America. *Crit Rev Microbiol* 36:1–53.

553 3. Slutsky B, Staebell M, Anderson J, Risen L, Pfaller M, Soll DR. 1987.
554 "White-opaque transition": a second high-frequency switching
555 system in *Candida albicans*. *J Bacteriol* 169:189–97.

556 4. Bennett RJ, Johnson a D. 2005. Mating in *Candida albicans* and the search
557 for a sexual cycle. *Annu Rev Microbiol* 59:233–55.

558 5. Kvaal C, Lachke SA, Srikantha T, Daniels K, McCoy J, Soll DR. 1999.
559 Misexpression of the opaque-phase-specific gene PEP1 (SAP1) in the white

560 phase of *Candida albicans* confers increased virulence in a mouse model of
561 cutaneous infection. *Infect Immun* 67:6652–62.

562 6. Kvaal CA, Srikantha T, Soll DR. 1997. Misexpression of the white-phase-
563 specific gene WH11 in the opaque phase of *Candida albicans* affects switching
564 and virulence. *Infect Immun* 65:4468–75.

565 7. Lachke SA, Lockhart SR, Daniels KJ, Soll DR. 2003. Skin facilitates *Candida*
566 *albicans* mating. *Infect Immun* 71:4970–6.

567 8. Huang G, Wang H, Chou S, Nie X, Chen J, Liu H. 2006. Bistable expression of
568 WOR1, a master regulator of white-opaque switching in *Candida albicans*.
569 *Proc Natl Acad Sci* 103:12813–12818.

570 9. Srikantha T, Borneman AR, Daniels KJ, Pujol C, Wu W, Seringhaus MR,
571 Gerstein M, Yi S, Snyder M, Soll DR. 2006. TOS9 Regulates White-Opaque
572 Switching in *Candida albicans*. *Eukaryot Cell* 5:1674–1687.

573 10. Zordan RE, Miller MG, Galgoczy DJ, Tuch BB, Johnson AD. 2007. Interlocking
574 Transcriptional Feedback Loops Control White-Opaque Switching in *Candida*
575 *albicans*. *PLoS Biol* 5:e256.

576 11. Zordan RE, Galgoczy DJ, Johnson AD. 2006. Epigenetic properties of white-
577 opaque switching in *Candida albicans* are based on a self-sustaining
578 transcriptional feedback loop. *Proc Natl Acad Sci U S A* 103:12807–12.

579 12. Miller MG, Johnson AD. 2002. White-opaque switching in *Candida albicans* is
580 controlled by mating-type locus homeodomain proteins and allows efficient
581 mating. *Cell* 110:293–302.

582 13. Noble SM, Gianetti BA, Witchley JN. 2017. *Candida albicans* cell-type

583 switching and functional plasticity in the mammalian host. *Nat Rev Microbiol*
584 15:96–108.

585 14. Staab JF, Bradway SD, Fidel PL, Sundstrom P. 1999. Adhesive and
586 mammalian transglutaminase substrate properties of *Candida albicans* Hwp1.
587 *Science* 283:1535–8.

588 15. Almeida RS, Brunke S, Albrecht A, Thewes S, Laue M, Edwards JE, Filler SG,
589 Hube B. 2008. The Hyphal-Associated Adhesin and Invasin Als3 of *Candida*
590 *albicans* Mediates Iron Acquisition from Host Ferritin. *PLoS Pathog*
591 4:e1000217.

592 16. Phan QT, Myers CL, Fu Y, Sheppard DC, Yeaman MR, Welch WH, Ibrahim
593 AS, Edwards JE, Filler SG. 2007. Als3 Is a *Candida albicans* Invasin That
594 Binds to Cadherins and Induces Endocytosis by Host Cells. *PLoS Biol* 5:e64.

595 17. Weissman Z, Kornitzer D. 2004. A family of *Candida* cell surface haem-binding
596 proteins involved in haemin and haemoglobin-iron utilization. *Mol Microbiol*
597 53:1209–1220.

598 18. Braun BR, Kadosh D, Johnson AD. 2001. NRG1, a repressor of filamentous
599 growth in *C. albicans*, is down-regulated during filament induction. *EMBO J*
600 20:4753–4761.

601 19. Lu Y, Su C, Wang A, Liu H. 2011. Hyphal Development in *Candida albicans*
602 Requires Two Temporally Linked Changes in Promoter Chromatin for Initiation
603 and Maintenance. *PLoS Biol* 9:e1001105.

604 20. Denning DW, Hope WW. 2010. Therapy for fungal diseases: opportunities and
605 priorities. *Trends Microbiol* 18:195–204.

606 21. Kurdistani SK, Grunstein M. 2003. Histone acetylation and deacetylation in
607 yeast. *Nat Rev Mol Cell Biol* 4:276–284.

608 22. Glazak MA, Sengupta N, Zhang X, Seto E. 2005. Acetylation and
609 deacetylation of non-histone proteins. *Gene* 363:15–23.

610 23. Haberland M, Montgomery RL, Olson EN. 2009. The many roles of histone
611 deacetylases in development and physiology: Implications for disease and
612 therapy. *Nat Rev Genet* 10:32–42.

613 24. Falkenberg KJ, Johnstone RW. 2014. Histone deacetylases and their inhibitors
614 in cancer, neurological diseases and immune disorders. *Nat Rev Drug Discov*
615 13:673–691.

616 25. Srikantha T, Tsai L, Daniels K, Klar AJS, Soll DR. 2001. The Histone
617 Deacetylase Genes HDA1 and RPD3 Play Distinct Roles in Regulation of
618 High-Frequency Phenotypic Switching in *Candida albicans*. *Society* 183:4614–
619 4625.

620 26. Hnisz D, Schwarzmüller T, Kuchler K. 2009. Transcriptional loops meet
621 chromatin: a dual-layer network controls white-opaque switching in *Candida*
622 *albicans*. *Mol Microbiol* 74:1–15.

623 27. Lu Y, Su C, Solis N V., Filler SG, Liu H. 2013. Synergistic regulation of hyphal
624 elongation by hypoxia, CO₂, and nutrient conditions controls the virulence of
625 *Candida albicans*. *Cell Host Microbe* 14:499–509.

626 28. Kadosh D, Lopez-Ribot JL. 2013. *Candida albicans*: Adapting to Succeed. *Cell*
627 *Host Microbe* 14:483–485.

628 29. Tzogani K, van Hennik P, Walsh I, De Graeff P, Folin A, Sjöberg J, Salmonson

629 T, Bergh J, Laane E, Ludwig H, Gisselbrecht C, Pignatti F. 2018. EMA Review
630 of Panobinostat (Farydak) for the Treatment of Adult Patients with Relapsed
631 and/or Refractory Multiple Myeloma. *Oncologist* 23:631–636.

632 30. Simó-Riudalbas L, Esteller M. 2015. Targeting the histone orthography of
633 cancer: drugs for writers, erasers and readers. *Br J Pharmacol* 172:2716–
634 2732.

635 31. Wu J, Carmen a a, Kobayashi R, Suka N, Grunstein M. 2001. HDA2 and
636 HDA3 are related proteins that interact with and are essential for the activity of
637 the yeast histone deacetylase HDA1. *Proc Natl Acad Sci U S A* 98:4391–6.

638 32. Lee JH, Maskos K, Huber R. 2009. Structural and Functional Studies of the
639 Yeast Class II Hda1 Histone Deacetylase Complex. *J Mol Biol* 391:744–757.

640 33. Shahana S, Childers DS, Ballou ER, Bohovych I, Odds FC, Gow N a R, Brown
641 AJP. 2014. New Clox Systems for rapid and efficient gene disruption in
642 *Candida albicans*. *PLoS One* 9:e100390.

643 34. Subramanian A, Tamayo P, Mootha VK, Mukherjee S, Ebert BL, Gillette MA,
644 Paulovich A, Pomeroy SL, Golub TR, Lander ES, Mesirov JP. 2005. Gene set
645 enrichment analysis: a knowledge-based approach for interpreting genome-
646 wide expression profiles. *Proc Natl Acad Sci U S A* 102:15545–50.

647 35. Sellam A, van het Hoog M, Tebaji F, Beaurepaire C, Whiteway M, Nantel A.
648 2014. Modeling the transcriptional regulatory network that controls the early
649 hypoxic response in *Candida albicans*. *Eukaryot Cell* 13:675–90.

650 36. Merico D, Isserlin R, Stueker O, Emili A, Bader GD. 2010. Enrichment Map: A
651 Network-Based Method for Gene-Set Enrichment Visualization and

652 Interpretation. PLoS One 5:e13984.

653 37. Enjalbert B, Nantel A, Whiteway M. 2003. Stress-induced gene expression in
654 *Candida albicans*: absence of a general stress response. Mol Biol Cell
655 14:1460–7.

656 38. Tuch BB, Mitrovich QM, Homann OR, Hernday AD, Monighetti CK, De La
657 Vega FM, Johnson AD. 2010. The transcriptomes of two heritable cell types
658 illuminate the circuit governing their differentiation. PLoS Genet 6:e1001070.

659 39. Breger J, Fuchs BB, Aperis G, Moy TI, Ausubel FM, Mylonakis E. 2007.
660 Antifungal Chemical Compounds Identified Using a *C. elegans* Pathogenicity
661 Assay. PLoS Pathog 3:e18.

662 40. Pukkila-Worley R, Peleg AY, Tampakakis E, Mylonakis E. 2009. *Candida*
663 *albicans* hyphal formation and virulence assessed using a *Caenorhabditis*
664 *elegans* infection model. Eukaryot Cell 8:1750–8.

665 41. Lewis RE, Kontoyiannis DP. 2001. Rationale for combination antifungal
666 therapy. Pharmacotherapy 21:149S–164S.

667 42. Homann OR, Dea J, Noble SM, Johnson AD. 2009. A phenotypic profile of the
668 *Candida albicans* regulatory network. PLoS Genet 5.

669 43. Gerami-nejad M, Forche A, McClellan M, Berman J. 2012. Analysis of protein
670 function in clinical *C. albicans* isolates 5314.

671 44. Park Y, Park Y, Morschhauser J, Morschhauser J. 2005. Tetracycline-
672 Inducible Gene Expression and Gene Deletion in *Candida albicans*.
673 Microbiology 4:1328–1342.

674 45. Gerami-Nejad M, Berman J, Gale CA. 2001. Cassettes for PCR-mediated

675 construction of green, yellow, and cyan fluorescent protein fusions in *Candida*
676 *albicans*. *Yeast* 18:859–864.

677 46. De Backer MD, Maes D, Vandoninck S, Logghe M, Contreras R, Luyten
678 WHML. 1999. Transformation of *Candida albicans* by Electroporation. *Yeast*
679 15:1609–1618.

680 47. Schiestl RH, Gietz RD. 1989. High efficiency transformation of intact yeast
681 cells using single stranded nucleic acids as a carrier. *Curr Genet* 16:339–346.

682 48. Knop M, Siegers K, Pereira G, Zachariae W, Winsor B, Nasmyth K, Schiebel
683 E. 1999. Epitope tagging of yeast genes using a PCR-based strategy: more
684 tags and improved practical routines. *Yeast* 15:963–972.

685 49. Walther A, Wendland J. 2003. An improved transformation protocol for the
686 human fungal pathogen *Candida albicans*. *Curr Genet* 42:339–343.

687 50. Kelley LA, Mezulis S, Yates CM, Wass MN, Sternberg MJE. 2015. The Phyre2
688 web portal for protein modeling, prediction and analysis. *Nat Protoc* 10:845–
689 58.

690 51. von der Haar T. 2007. Optimized protein extraction for quantitative proteomics
691 of yeasts. *PLoS One* 2:e1078.

692 52. Buscaino A, White SA, Houston DR, Lejeune E, Simmer F, de Lima Alves F,
693 Diyora PT, Urano T, Bayne EH, Rappaport J, Allshire RC. 2012. Raf1 Is a
694 DCAF for the Rik1 DDB1-Like Protein and Has Separable Roles in siRNA
695 Generation and Chromatin Modification. *PLoS Genet* 8:e1002499.

696 53. Pathan M, Keerthikumar S, Chisanga D, Alessandro R, Ang C-S, Askenase P,
697 Batagov AO, Benito-Martin A, Camussi G, Clayton A, Collino F, Di Vizio D,

698 Falcon-Perez JM, Fonseca P, Fonseka P, Fontana S, Gho YS, Hendrix A,
699 Hoen EN-'t, Iraci N, Kastaniegaard K, Kislinger T, Kowal J, Kurochkin I V.,
700 Leonardi T, Liang Y, Llorente A, Lunavat TR, Maji S, Monteleone F, Øverbye
701 A, Panaretakis T, Patel T, Peinado H, Pluchino S, Principe S, Ronquist G,
702 Royo F, Sahoo S, Spinelli C, Stensballe A, Théry C, van Herwijnen MJC,
703 Wauben M, Welton JL, Zhao K, Mathivanan S. 2017. A novel community
704 driven software for functional enrichment analysis of extracellular vesicles
705 data. *J Extracell Vesicles* 6:1321455.

706 54. Mootha VK, Lindgren CM, Eriksson K-F, Subramanian A, Sihag S, Lehar J,
707 Puigserver P, Carlsson E, Ridderstråle M, Laurila E, Houstis N, Daly MJ,
708 Patterson N, Mesirov JP, Golub TR, Tamayo P, Spiegelman B, Lander ES,
709 Hirschhorn JN, Altshuler D, Groop LC. 2003. PGC-1alpha-responsive genes
710 involved in oxidative phosphorylation are coordinately downregulated in human
711 diabetes. *Nat Genet* 34:267–73.

712 55. Sellam A, Hogues H, Askew C, Tebbji F, van Het Hoog M, Lavoie H,
713 Kumamoto C a, Whiteway M, Nantel A. 2010. Experimental annotation of the
714 human pathogen *Candida albicans* coding and noncoding transcribed regions
715 using high-resolution tiling arrays. *Genome Biol* 11:R71.

716 56. Shannon P, Markiel A, Ozier O, Baliga NS, Wang JT, Ramage D, Amin N,
717 Schwikowski B, Ideker T. 2003. Cytoscape: A Software Environment for
718 Integrated Models of Biomolecular Interaction Networks. *Genome Res*
719 13:2498–2504.

720 57. Moy TI, Ball AR, Anklesaria Z, Casadei G, Lewis K, Ausubel FM. 2006.
721 Identification of novel antimicrobials using a live-animal infection model. *Proc*

722 Natl Acad Sci U S A 103:10414–10419.

723 58. Han SK, Lee D, Lee H, Kim D, Son HG, Yang J-S, Lee S-J V., Kim S. 2016.

724 OASIS 2: online application for survival analysis 2 with features for the

725 analysis of maximal lifespan and healthspan in aging research. Oncotarget

726 7:56147–56152.

727 59. Synnott JM, Guida A, Mulhern-Haughey S, Higgins DG, Butler G. 2010.

728 Regulation of the Hypoxic Response in *Candida albicans*. Eukaryot Cell

729 9:1734–1746.

730 60. Marcil A, Gadoury C, Ash J, Zhang J, Nantel A, Whiteway M. 2008. Analysis of

731 PRA1 and its relationship to *Candida albicans*-macrophage interactions. Infect

732 Immun 76:4345–4358.

733 61. Noble SM, Johnson AD. 2005. Strains and Strategies for Large-Scale Gene

734 Deletion Studies of the Diploid Human Fungal Pathogen *Candida albicans*

735 Eukaryot Cell 4: 298-309

736 62. Wilson RB, Davis D, Mitchell AP. 1999. Rapid Hypothesis Testing with

737 *Candida albicans* through Gene Disruption with Short Homology Regions

738 Journal of bacteriology 181: 1868-74

739

740

741 **FIGURE LEGENDS**

742 **Figure 1. The Hda1 complex is conserved in *C. albicans***

743 **(A)** Domain organisation of *C. albicans* Hda2 and Hda3 proteins **(B)** *Left:* Structural
744 alignment of *C. albicans* DBD3 domain (red) with *S. cerevisiae* DBD3 domain

745 (yellow); *Right*: Structural modelling of *C. albicans* CCD3 (**C**) Co-
746 Immunoprecipitation of Hda1 with Hda2 and Hda3. Hda1-HA Immunoprecipitation
747 (Ip) analysed with anti-HA or with anti-GFP to detect Hda2 and Hda3. (**D**) Schematic
748 of *Clox* gene disruption strategy used to construct *hda2Δ/Δ* and *hda3Δ/Δ* mutants.
749 (**E**) Serial dilution assay of WT, *hda2Δ/Δ* and *hda3Δ/Δ* mutants on solid YPD media
750 at 30 °C. (**F**) Growth curves of WT, *hda2Δ/Δ* and *hda3Δ/Δ* isolates in YPD liquid
751 media at 30 °C.

752

753 **Figure 2. Global gene expression changes in the absence of Hda2 and Hda3**

754 (**A**) Pearson correlation matrix of gene expression changes observed in *hda1 Δ/Δ*,
755 *hda2 Δ/Δ* and *hda3 Δ/Δ* grown in YPD at 30 °C. r = Pearson correlation coefficient. p
756 = p-value. (**B**) The network of functional groups of genes regulated by Hda2 and
757 Hda3 constructed by GSEA and Enrichment Map. Blue circles represent down
758 regulated while orange circles depict upregulated gene sets which are linked in the
759 network by grey lines. The diameter of the circles varies based upon the number of
760 transcripts within each set. (**C**) Example enrichment plots for selected genes sets
761 differentially expressed in *hda2 Δ/Δ* (left) and *hda3 Δ/Δ* (right). Ketoconazole_up: set
762 of genes upregulated in *C. albicans* cells grown in the presence of ketoconazole
763 (59); Phagocytosis_up: gene set upregulated following engulfment by primary Bone
764 Marrow Derived Macrophages (60). The x-axis shows genes ranked according to
765 their expression in the mutants from up-regulated (left) to down-regulated (right)
766 genes. Black vertical lines mark individual genes. The cumulative value of the
767 enrichment score (y-axis) is represented by the green line. A positive normalised
768 enrichment score (NES) indicates enrichment in the up-regulated group of genes in
769 *hda2 Δ/Δ* and *hda3 Δ/Δ*.

770 **Figure 3. Phenotyping of *hda2* Δ/Δ and *hda3* Δ/Δ strains**

771 Serial dilution assay showing growth of *hda2* Δ/Δ and *hda3* Δ/Δ mutants on solid
772 YPD media with additives as indicated and incubation at 30 °C for 2 - 4 days. **(A)**
773 Additives affecting *hda2* Δ/Δ and *hda3* Δ/Δ growth relative to wildtype strain. Mutants
774 are resistant to rapamycin and sensitive to SNP and SHAM, sodium chloride and
775 copper sulphate. **(B)** Conditions eliciting normal growth of mutant strains relative to
776 matching wildtype.

777 **Figure 4. Hda2 and Hda3 inhibit white-opaque switching**

778 **(A)** Enrichment plots for genes differentially expressed in *hda1* Δ/Δ, *hda2* Δ/Δ and
779 *hda3* Δ/Δ in comparison to genes upregulated in opaque cells (38). The x-axis shows
780 genes ranked according to their expression in the mutants from up-regulated (left) to
781 down-regulated (right) genes. Black vertical lines mark individual genes. The
782 cumulative value of the enrichment score (y-axis) is represented by the green line. A
783 positive normalised enrichment score (NES) indicates enrichment in the up-regulated
784 group of genes in *hda1* Δ/Δ, *hda2* Δ/Δ and *hda3* Δ/Δ. **(B)** Heat map depicting the log2
785 fold change in *hda1* Δ/Δ, *hda2* Δ/Δ and *hda3* Δ/Δ isolates compared to WT for the
786 Opaque_up gene set. **(C)** Log2 fold change values and significance for *WOR1* gene
787 expression in *hda1* Δ/Δ, *hda2* Δ/Δ and *hda3* Δ/Δ compared to WT. **(D) Left:**
788 Percentage of sector colonies in WT, *hda2* Δ/Δ and *hda3* Δ/Δ isolates. ** = p value ≤
789 .01. **Right:** Representative image of cells grown on Phloxine B agar. O = opaque; W
790 = white.

791 **Figure 5. Gene expression profiling in hyphae-inducing conditions in WT, *hda1*
792 Δ/Δ, *hda2* Δ/Δ and *hda3* Δ/Δ isolates**

793 (A) The network representing changes in gene expression in WT cells grown in
794 yeast-inducing conditions (YPD) versus hyphae-inducing conditions (RPMI)
795 constructed by GSEA and Enrichment Map. Blue circles represent down regulated
796 gene sets, while orange depicts upregulated gene sets which are linked in the
797 network by grey lines that indicate function. The diameter of the circles varies based
798 upon the number of transcripts within each set. (B) Pearson correlation matrix of
799 gene expression changes observed in *hda1* Δ/Δ, *hda2* Δ/Δ and *hda3* Δ/Δ grown in in
800 hyphae growth media (RPMI) at 37 °C. r = Pearson correlation coefficient. p = p-
801 value. (C) Left: Heat map depicting the log2 fold change in WT cells grown in
802 hyphae-inducing conditions (RPMI at 37 °C) versus WT cells grown in yeast-inducing
803 conditions (YPD at 30 °C). Gene known to be involved in hyphae formation or biofilm
804 formation are indicated. Right: Log2 fold changes of hyphae-induced and repressed-
805 genes in *hda1* Δ/Δ, *hda2* Δ/Δ and *hda3* Δ/Δ isolates. Cell were grown in RPMI at 37
806 °C. (D) Quantitative reverse transcriptase PCR (qRT-PCR) analyses to measure
807 *HWP1* and *ALS3* transcript levels in WT, *hda1* Δ/Δ, *hda2* Δ/Δ and *hda3* Δ/Δ isolates
808 grown in yeast (YPD at 30 °C) or hyphae (RPMI at 37 °C) inducing conditions.
809 Transcripts levels are visualized relative to *ACT1* transcript levels. Error bars in each
810 panel: standard deviation of three biological replicates.

811 **Figure 6. Hda2 and Hda3 contribute to filamentation growth but not virulence**
812 (A) Left: Representative images of colony morphology of WT, *hda1* Δ/Δ, *hda2* Δ/Δ
813 and *hda3* Δ/Δ grown on hyphal inducing Spider and RPMI agar at 37 °C. Right:
814 Quantification of colony morphologies. (B) Quantification of cellular morphologies of
815 WT, *hda1* Δ/Δ, *hda2* Δ/Δ and *hda3* Δ/Δ grown in liquid RPMI media at 37 °C. (C)
816 Rescue experiment of colony morphology upon genomic integration of the *HDA3*
817 gene in the *hda3* Δ/Δ mutant background (*hda3* Δ/Δ+ *HDA3*). WT, heterozygous

818 (*HDA3/ hda3* Δ) and homozygous *hda3* Δ/Δ isolates were included as a control. Cell
819 were grown on hyphal inducing RPMI agar at 37 °C. **(D)** *Left*: Representative images
820 of dead *C. elegans* with and without hyphae-mediated killing. *Middle*: Survival curve
821 of worms incubated with WT, *hda2* Δ/Δ and *hda3* Δ/Δ strains over a 72 hour period.
822 *Right*: The percentage of total worms dead (black bars) and worms killed by hyphae
823 piercing the cuticle (grey bars) after the 72 hour incubation period. Error bars
824 represent the standard deviation of three independent biological replicates.

825 **Figure 7. Stability of the Hda1 protein is regulated by environmental changes**

826 **(A)** Venn diagram of genes differentially expressed in *hda1* Δ/Δ relative to WT in
827 yeast and hyphal growth conditions. **(B)** Enrichment plots for genes differentially
828 expressed in *hda1* Δ/Δ relative to genes downregulated (Hyphae_Lee_DN) or
829 upregulated (Hyphae_Lee_up) in hyphae-growth condition in Lee's media . The x-
830 axis shows genes ranking according to their expression in *hda1* Δ/Δ from up-
831 regulated (left) to down-regulated (right) genes. Black vertical lines mark individual
832 genes. The cumulative value of the enrichment score (y-axis) is represented by the
833 green line. A positive normalised enrichment score (NES) indicates enrichment in the
834 up-regulated group of genes while a negative NES indicates prevalence of the genes
835 in the down-regulated group. **(C)** HA and GFP Western blots of whole protein extract
836 from strains: Hda1-HA, Hda2-GFP and Hda3-GFP. Actin is shown as a loading
837 control. Cells were grown in yeast (YPD 30 °C) or hyphae-inducing (RPMI 37 °C)
838 conditions. **(D)** Model showing how decreased Hda1 and Hda3 protein levels leading
839 to the functional rewiring of the Hda1 complex in *C. albicans* in different
840 environments. Under yeast growth condition, the Hda1 complex functions as a global
841 regulator of gene expression due to the high level of Hda1 and Hda3. Under hyphae

842 growth conditions, decreased levels of Hda1 and Hda3 leads to specialisation of the
843 Hda1 complex controlling only filamentous growth.

844

845 **Table 1.** *C.albicans* strains used in this study.

Strain Number	Description	Genotype	Figure	Source
ABy_54	SN152	<i>MTL a/alpha ura3Δ- iro1Δ::imm434/URA3-IRO1 his1Δ/his1Δ arg4Δ/arg4Δ leu2Δ/leu2Δ</i>	1E-F, 2A-C, 3A-B, 4A-C, 5A-D, 6A-B, 6D, 7A-B	(61)
ABy_66	BWP17	<i>MTL a/alpha ura3Δ::Δimm434/ura3Δ::Δi mm434 his1::hisG/his1::hisG arg4::hisG/arg4::hisG</i>	1F, 6B-C	(62)
ABy_179	<i>hda1 Δ/Δ</i>	<i>MTL a/a arg4Δ/arg4Δ his1Δ/his1Δ leu2Δ/leu2Δ URA3/ura3Δ::λimm434IRO1 /iro1Δ::λimm434 hda1Δ::C.d.HIS1/hda1Δ::C. m.LEU2</i>	2A-C, 3A-B, 4A-C, 5A-D, 6A-B, 6D, 7A-B	(26)
ABy_191	<i>HDA3/Δ</i>	<i>MTL a/alpha ura3Δ::Δimm434/ura3Δ::Δi mm434 his1::hisG/his1::hisG arg4::hisG/arg4::hisG HDA3/hda3Δ::LAL</i>	6C	This study
ABy_331	<i>BWP17 hda3Δ/Δ</i>	<i>MTL a/alpha ura3Δ::Δimm434/ura3Δ::Δi mm434 his1::hisG/his1::hisG arg4::hisG/arg4::hisG hda3Δ/hda3Δ</i>	1F, 6B-C	This study
ABy_347	<i>hda2Δ/Δ</i>	<i>MTL a/alpha ura3Δ- iro1Δ::imm434/URA3-IRO1 his1Δ/his1Δ arg4Δ/arg4Δ leu2Δ/leu2Δ hda2Δ/hda2Δ</i>	1E-F, 2A-C, 3A-B, 4A-D, 5A-C, 6B, 6D, 6A	This study
ABy_376	<i>HDA3:HDA3-GFP</i>	<i>MTL a/alpha ura3Δ::Δimm434/ura3Δ::Δi mm434 his1::hisG/his1::hisG arg4::hisG/arg4::hisG HDA3::HIS/HDA3-GFP</i>	1C, 7C	This study
ABy_393	<i>BWP17 MTLαΔ</i>	<i>MTLa/MTLαΔ ura3Δ::Δimm434/ura3Δ::Δi mm434 his1::hisG/his1::hisG arg4::hisG/arg4::hisG</i>	4D	This study

ABy_460	SN152 <i>hda3Δ/Δ</i>	<i>MTL a/alpha ura3Δ- iro1Δ::imm434/URA3-IRO1 his1Δ/his1Δ arg4Δ/arg4Δ leu2Δ/leu2Δ hda3Δ/hda3Δ</i>	1E, 2A-C, 3A-B, 4A-C, 5A-D, 6A-B, 6D	This study
ABy_472	<i>ADH1/ pNIM- HDA3:adh1Δ</i>	<i>MTL a/alpha ura3Δ::Δimm434/ura3Δ::Δi mm434 his1::hisG/his1::hisG arg4::hisG/arg4::hisG hda3Δ/hda3Δ pNIM- HDA3::adh1Δ/ADH1</i>	6C	This study
ABy_532	<i>HDA2:HDA2- GFP</i>	<i>MTL a/alpha ura3Δ::Δimm434/ura3Δ::Δi mm434 his1::hisG/his1::hisG arg4::hisG/arg4::hisG HDA2::HIS/HDA2-GFP</i>	1C, 7C	This study
ABy_536	<i>HDA2:HDA2- GFP HDA1:HDA1- HA</i>	<i>MTL a/alpha ura3Δ::Δimm434/ura3Δ::Δi mm434 his1::hisG/his1::hisG arg4::hisG/arg4::hisG HDA2::HIS/HDA2-GFP HDA1::NAT/HDA1-HA</i>	1C	This study
ABy_539	<i>HDA3:HDA3- GFP HDA1:HDA1- HA</i>	<i>MTL a/alpha ura3Δ::Δimm434/ura3Δ::Δi mm434 his1::hisG/his1::hisG arg4::hisG/arg4::hisG HDA3::HIS/HDA3-GFP HDA1::NAT/HDA1-HA</i>	1C	This study
ABy_547	<i>hda2Δ/Δ MTLαΔ</i>	<i>MTL a/ MTLalphaΔ ura3Δ- iro1Δ::imm434/URA3-IRO1 his1Δ/his1Δ arg4Δ/arg4Δ leu2Δ/leu2Δ hda2Δ/hda2Δ</i>	4D	This study
ABy_551	<i>hda3Δ/Δ MTLαΔ</i>	<i>MTL a/ MTLalphaΔ ura3Δ- iro1Δ::imm434/URA3-IRO1 his1Δ/his1Δ arg4Δ/arg4Δ leu2Δ/leu2Δ hda3Δ/hda3Δ</i>	4D	This study
ABy_563	<i>HDA1:HDA1- HA</i>	<i>MTL a/alpha ura3Δ::Δimm434/ura3Δ::Δi mm434 his1::hisG/his1::hisG arg4::hisG/arg4::hisG HDA1::NAT/HDA1-HA</i>	1C, 7C	This study

846

847 **Table 2.** Oligos used in this study.

Number	Primer	Sequence	Figure	Description
ABo_408	HDA1_Xma_fw1	TAAGCACCCGGGatgt cgactggtaagaagaa	1C, 7C-D	Isolate synthetic Hda1 from p88
ABo_409	HDA1_Xma_rev1	TAAGCACCCGGGatctt	1C, 7C-D	Isolate synthetic Hda1

		cggaagaggagtagtc		from p88
ABo_351	Pr_sir2_adh1	CGCACTCACGTAAC ACTT	1C, 6C, 7C-D	Check Hda1 in p17; confirm reintegration of Hda3_pNIM cassette at ADH1 locus
ABo_412	HDA1end_chkseq	GGAAATAGTTCGAAC GGTGG	1C, 7C-D	Check Hda1 in p17; sequencing p133
ABo_452	F1gaHDA1_Haintg	TCCGAAATTCAATTATT AAGGAATTATATAGA AGCTACCATTTCAC ATCTATTATCATTTC CTTTTTAAGAatgtcgact ggtaagaagaaca	1C, 7C-D	Isolate Hda1-HA integration cassette from p133; long oligo
ABo_453	R1gaHDA1_Haintg	CAGATCTATATCTATT CTCTTTCTTTCTTTTT TTTGGTTTTTTGTTG TTGTTGTTGTTGTTTC TACTCGAAgtaaaacga cgcccaagtgaattc	1C, 7C-D	Isolate Hda1-HA integration cassette from p133; long oligo
ABo_179	PR1_NAT	CTGTATCTATAAGCA GTATCATCC	1C, 7C-D	Check presence of Hda1-HA integration cassette at native locus
ABo_417	dwnstrmHDA1rev_ check	CTCGATGCCTGATT GGATG	1C, 7C-D	Check presence of Hda1-HA integration cassette at native locus
ABo_458	F1HDA2_GFP	TGTTAGAAAACTCTG GCTCGGGTGCCAATA ATAGACAAAATAATC GTATTAGTCGAGGTG CAACACCTCTGGTG GTGGTtctaaaggtaaga attatt	1C, 7C-D	Isolate GFP tagging cassette from p11 with flanking integration sequences for Hda2; long oligo
ABo_459	R2HDA2_GFP	GCATGTATTTACAAA TTTTGGATAAGAAA AAGTAGCATATGGAA ACACAAAACCAAGAA AGAAATCATGgaattcc ggaatatttatgagaaac	1C, 7C-D	Isolate GFP tagging cassette from p11 with flanking integration sequences for Hda2; long oligo
ABo_460	F1HDA3_GFP	CAATGCTTTACATT TTAAATGATACTAAAT ATTGAAAAAGAGGA AAAATCGAGGAATAA CTCCTAAAGGTGGTG GTtctaaaggtaagaattatt	1C, 7C-D	Isolate GFP tagging cassette from p11 with flanking integration sequences for Hda3; long oligo
ABo_461	R2HDA3_GFP	CTTATCATTTACATAA TTAAAAAAACAAAAAA ACAAGCTAATCTTAT GTTTATGTGGGGGCC ACATTTCTgaattccgg aatatttatgagaaac	1C, 7C-D	Isolate GFP tagging cassette from p11 with flanking integration sequences for Hda3; long oligo
ABo_145	PF1_his1	GTTCCAGCAGATGGC	1C, 7C-D	Check Hda3-GFP or

		GAGTAC		Hda2-GFP tagging
ABo_261	Pr4_hda2chk_rev	GTAATATCTGATCAG AACCTTT	1C, 7C-D	Check Hda2-GFP tagging
ABo_262	Pr4_hda3chk_rev	TCGTTAACAAATTAA TACACTC	1C, 7C-D	Check Hda3-GFP tagging
ABo_229	HDA2D_Clox_Fw1	TCTATTTCAAGAAGT TAGACCCATTCTGG AATAATTATACTTGCA AGAGAAGGCATTGAA ATTGCATTACGGCCA GTGAATTGTAATA	1D	Isolate deletion cassette from p80 or p83 with flanking integration sequences for Hda2; long oligo
ABo_230	HDA2D_Clox_rev1	GCATGTATTTACAAA TTTTGGATAAGAAA AAGTAGCATATGGAA ACACAAAACCAAGAA AGAAATCATGTCGGA ATTAACCCCTCACTAA	1D	Isolate deletion cassette from p80 or p83 with flanking integration sequences for Hda2; long oligo
ABo_165	Pr1_chk_arg4	AGTGTGGAAAGAAGA GATGC	1D	Check presence of p80 cassette in Hda2 or Hda3 heterozygote
ABo_423	HDA3_Natcloxchk	CCGGTGCTATGGTTA GATTG	1D	Check presence of p83 cassette in hda2 $\Delta\Delta$ or hda3 $\Delta\Delta$
ABo_261	Pr4_hda2chk_rev	GTAATATCTGATCAG AACCTTT	1D	Check presence of p80 cassette in Hda2 heterozygote and hda2 $\Delta\Delta$
ABo_413	HDA2chk_internalfw	CAGCAGGTAGACTTG ATG	1D	Check presence/absence of Hda2 in hda2 $\Delta\Delta$ unresolved/resolved
ABo_261	Pr4_hda2chk_rev	GTAATATCTGATCAG AACCTTT	1D	Check presence/absence of Hda2 in hda2 $\Delta\Delta$ unresolved/resolved
ABo_231	HDA3D_Clox_Fw1	GTTCTTAATATTTGTA ACTTTCCAACCTAAA ATAATTATTGCATATT GCACTAAAACAAAA CTACTATAAAATacggcc agtgaattgtataata	1D	Isolate deletion cassette from p80 or p83 with flanking integration sequences for Hda3; long oligo
ABo_232	HDA3D_Clox_Rev1	CAATCTTATCATTAC ATAATTAACAAACAA AAAACAAGCTAATCT TATGTTTATGTGGGG GCCACATTCTtcgga attaaccctactaa	1D	Isolate deletion cassette from p80 or p83 with flanking integration sequences for Hda3; long oligo
ABo_262	Pr4_hda3chk_rev	TCGTTAACAAATTAA TACACTC	1D	Check presence of p80 or p83 cassette in Hda3 heterozygote or hda3 $\Delta\Delta$
ABo_415	HDA3chk_internalfw	CAACAAGAAcTGTGG AACATG	1D	Check presence/absence of Hda3 in hda3 $\Delta\Delta$

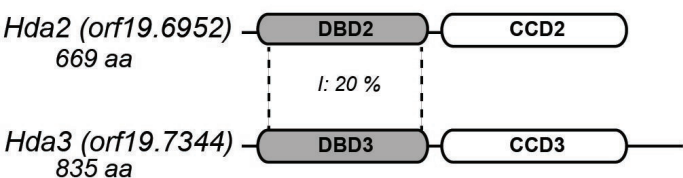
				unresolved/resolved
ABo_416	HDA3chk_internalrev	GGTGGTTCTATAAAT CCCGG	1D	Check presence/absence of Hda3 in hda3 $\Delta\Delta$ unresolved/resolved
ABo_462	Pf_MTLa1_Chk	TTGAAGCGTGAGAG GCAGGAG	4D	Check presence of MAT α
ABo_463	Pr_MTLa1_Chk	GTTCGGGTTCCCTCT TTCTCATTC	4D	Check presence of MAT α
ABo_464	Pf_MTLalpha1_Chk	TTCGAGTACATTCTG GTCGCG	4D	Check presence of MAT α
ABo_465	Pr_MTLalpha1_Chk	TGTAACACATCCTCAA TTGTACCCGA	4D	Check presence of MAT α
ABo_511	Pf_SAT1	GGTGGCGGAAACATT GGATG	4D	Check presence of Sat1
ABo_512	Pr_SAT1	TCAATGCCGCCGAGA GTAAA	4D	Check presence of Sat1
ABo_624	HDA3_Xhol_fw	TAAGCACTCGAGATG gattaaggaaaatttg	6C	Isolate Hda3 from ABp152 with Xhol and BgIII sites (for cloning into ABp111)
ABo_625	HDA3_stpBgIII_rev	TTAACGAGATCTttttta ggagttttccctcgat	6C	Isolate Hda3 from ABp152 with Xhol and BgIII sites (for cloning into ABp111: pNIM)
ABo_416	HDA3chk_internalrev	GGTGGTTCTATAAAT CCCGG	6C	Confirm cloning of p177 (Hda3_pNIM)
ABo_514	pNIM_Rev2	CAGTTGGTTCAGCA CCTTG	6C	Confirm cloning of ABp_177 (Hda3_pNIM)
LD_515		CCATCATAAAATGTC GAGCGTC	6C	Sequencing of ABp_177 (Hda3_pNIM)
ABo_350	Pf_sir2_adh1	ctctatcactgatagggagtg	6C	Confirm reintegration of ABp_177 (Hda3_pNIM) cassette at ADH1 locus
ABo_174	Act1_Fw2	CTACGTTCCATTCA AGCTGTT	5D	qRT-PCR for ACT1
ABo_176	Act1_Rev3	AAACTGTAACCACGT TCAGACA	5D	qRT-PCR for ACT1
ABo_469	qALS3_Fw1	CCTATTCCAACAACT ACAAT	5D	qRT-PCR for ALS3
ABo_470	qALS3_Rev1	TATTGAGTCAGTTGG ATTAG	5D	qRT-PCR for ALS3
ABo_471	qHWP1_Fw1	CCAGTTACTTCTGGA TCATC	5D	qRT-PCR for HWP1
ABo_472	qHWP1_Rev1	TCGGTACAAACACTG TTAGA	5D	qRT-PCR for HWP1

850 **Table 3.** Plasmids used in this study.

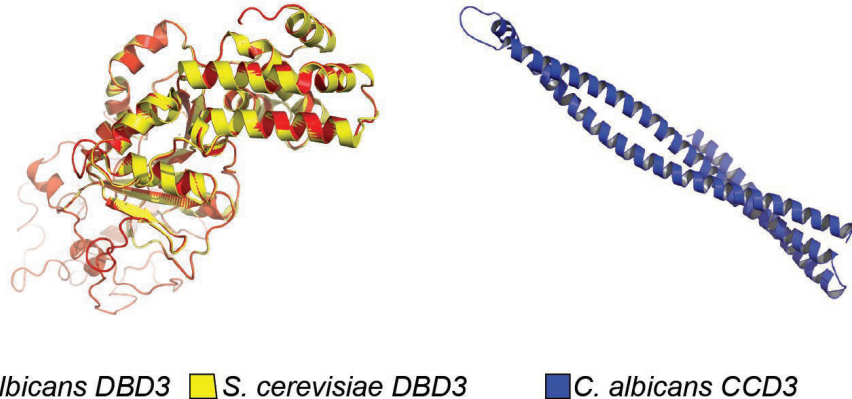
ABp_Number	Plasmid	Figure	Description/Source	Source
ABp_11	pGFP-His1	1C	GFP tagging vector	(45)
ABp_17	pHA_NAT1	1C	HA tagging vector	(43)
ABp_80	LAL (loxP-ARG4-loxP)	1D	<i>Arg4</i> substitution products	(33)
ABp_83	NAT1-Clox (loxP-NAT1-MET3p-cre-loxP)	1D	<i>Nat</i> substitution products	(33)
ABp_88	HDA1_syntheti c	1C	Hda1 synthetic	GeneArt
ABp_111	pNIM	6C	Tetracycline inducible integration to ADH1 locus	(44)
ABp_133	HDA1synthetic _pHA_NAT	1C	Source of Hda1-HA integration cassette	This study
ABp_136	Sat1 flipper with MTL α KO flanking regions	4D	Deletion of MAT α	Gift from Matthew Anderson Lab, Ohio State
ABp_152	HDA3 synthetic	6C	HA-HDA3 synthetic: 6x CUG->TCA	GeneArt
ABp_177	HDA3-pNIM	6C	Tetracycline inducible integration of Hda3 to ADH1 locus	This study

851

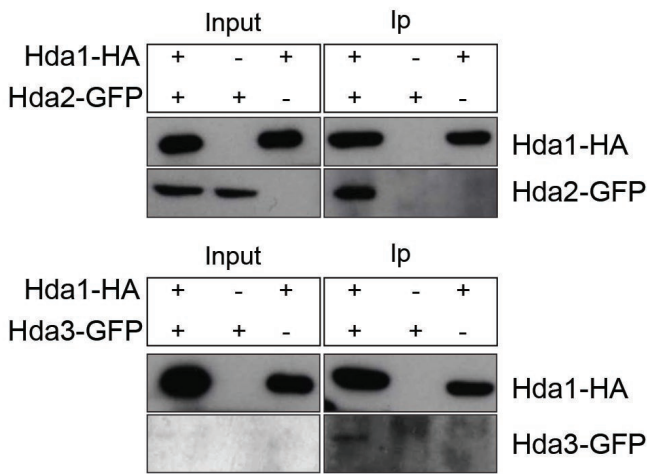
A



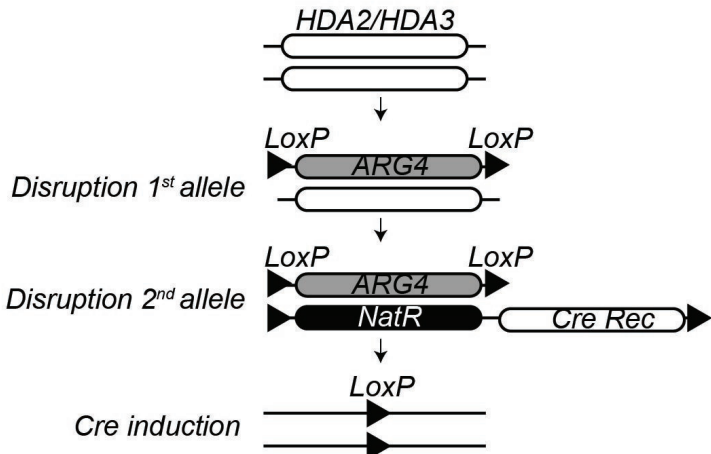
B



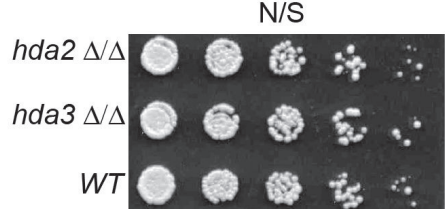
C



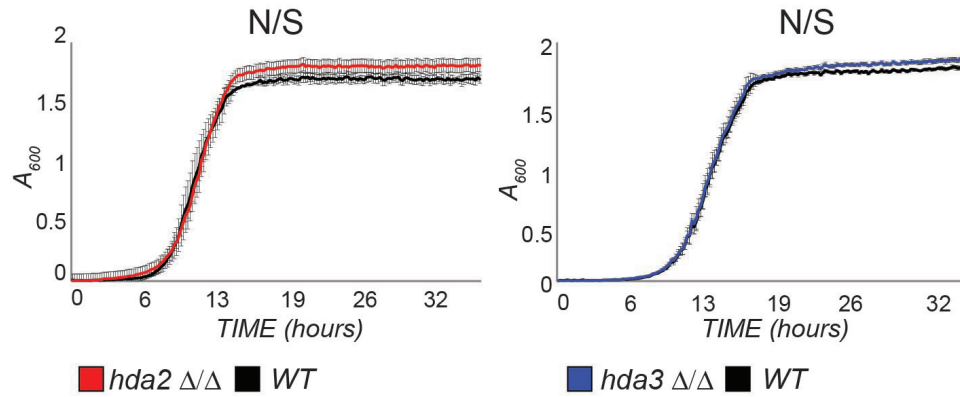
D

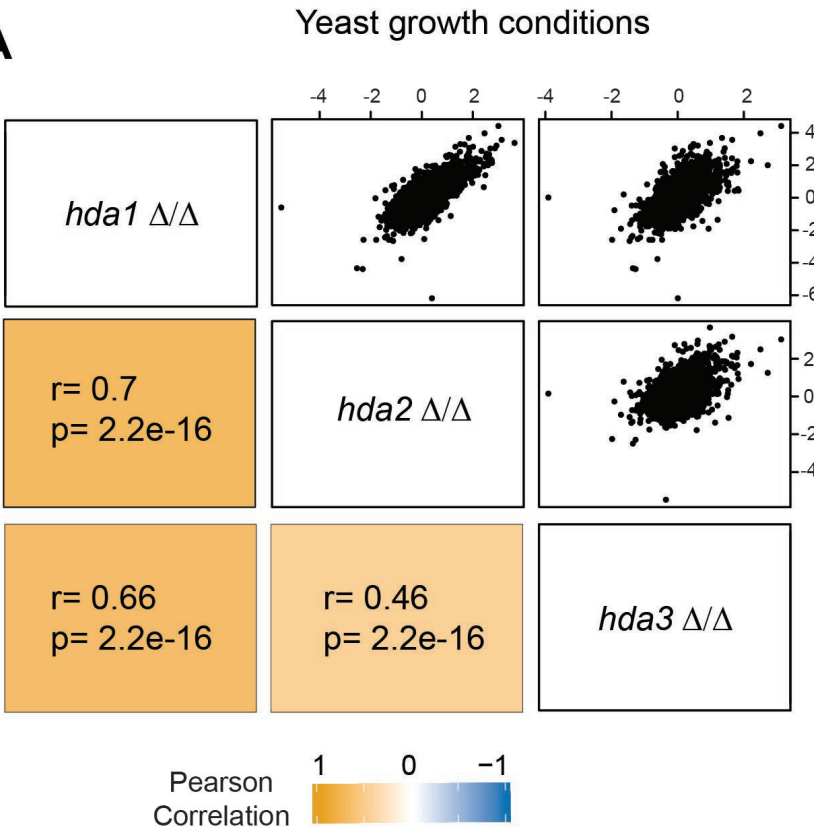
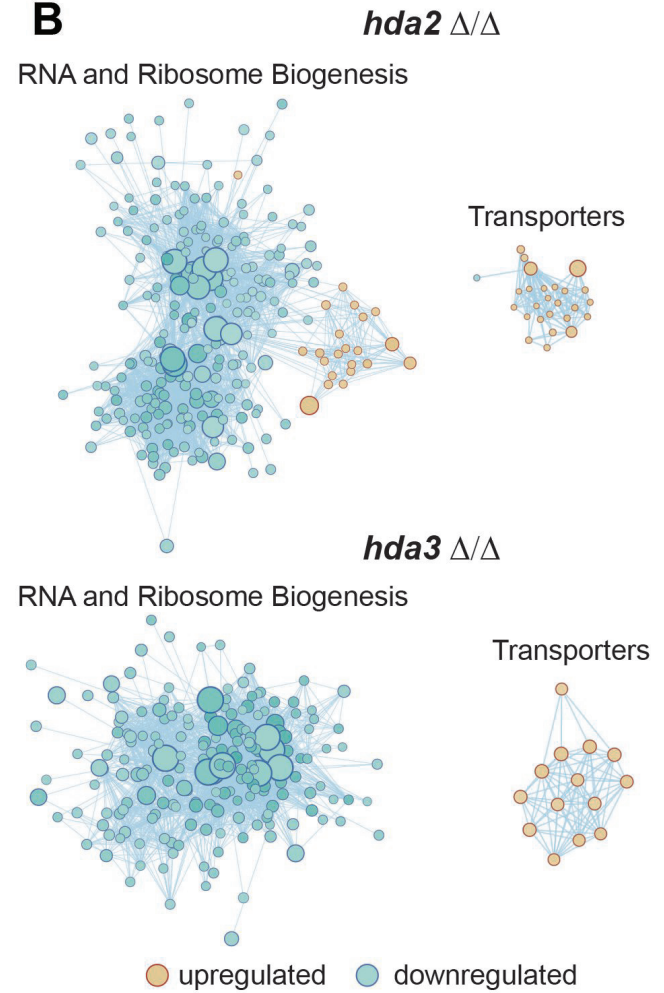


E

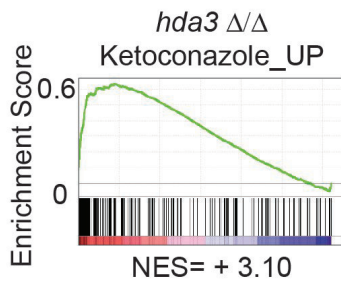
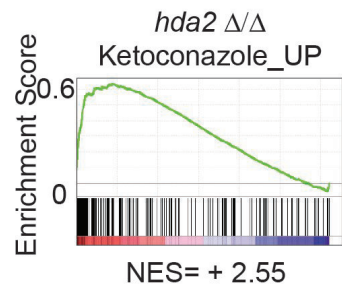


F

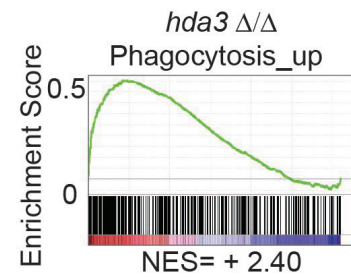
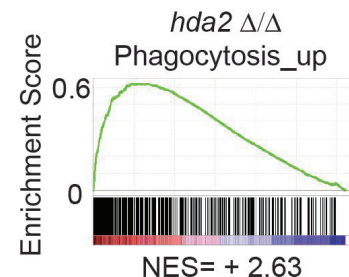


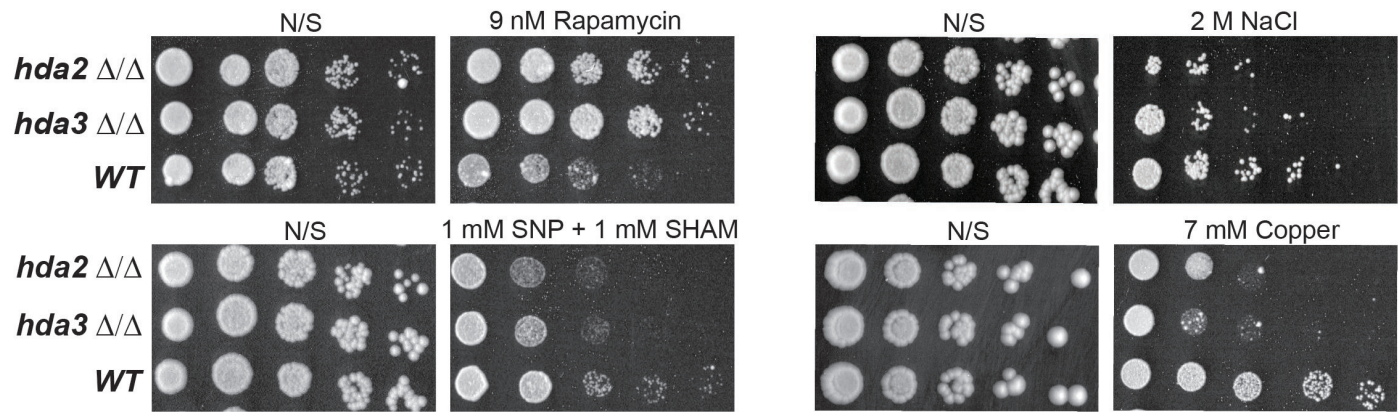
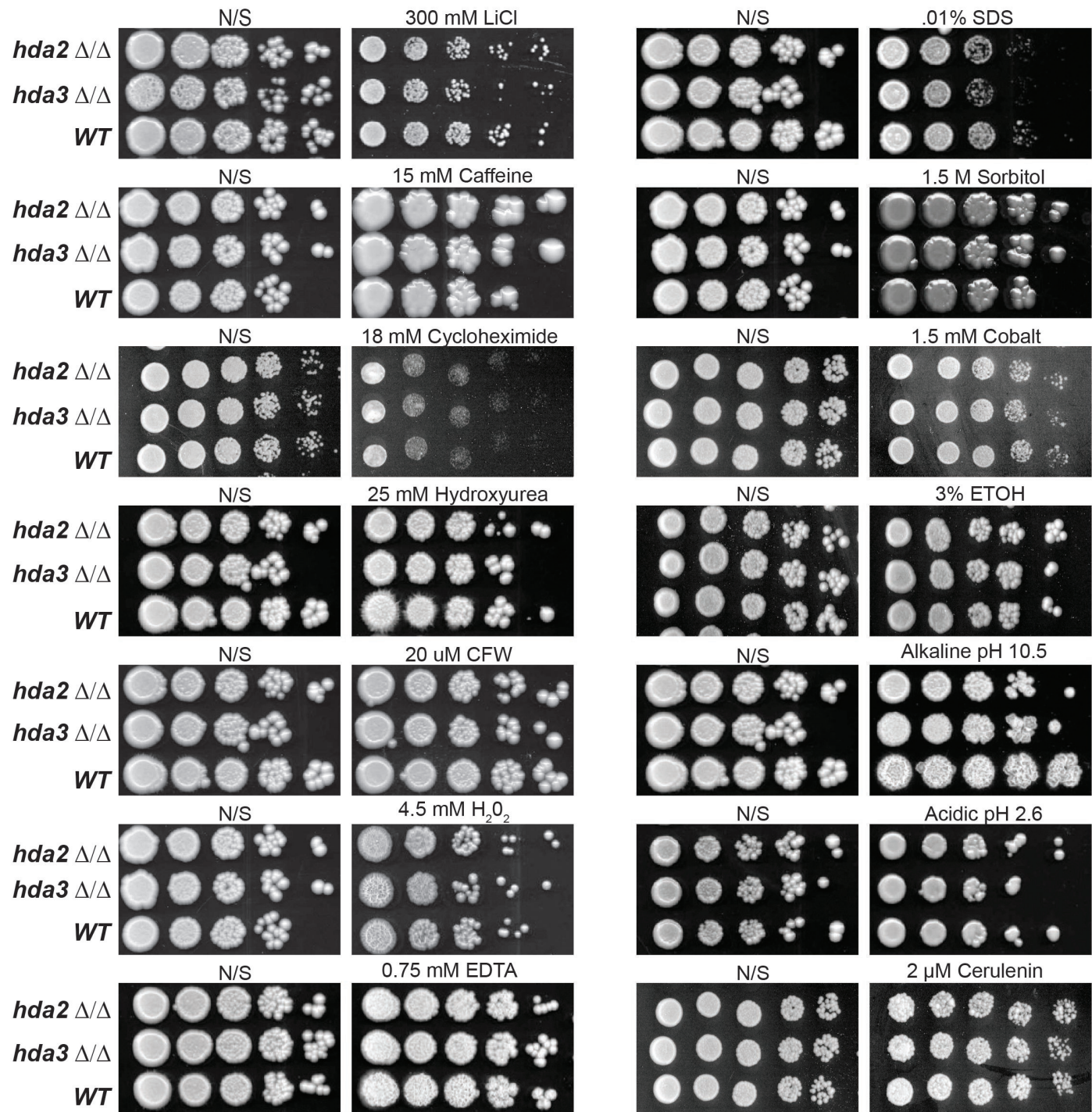
A**B****C**

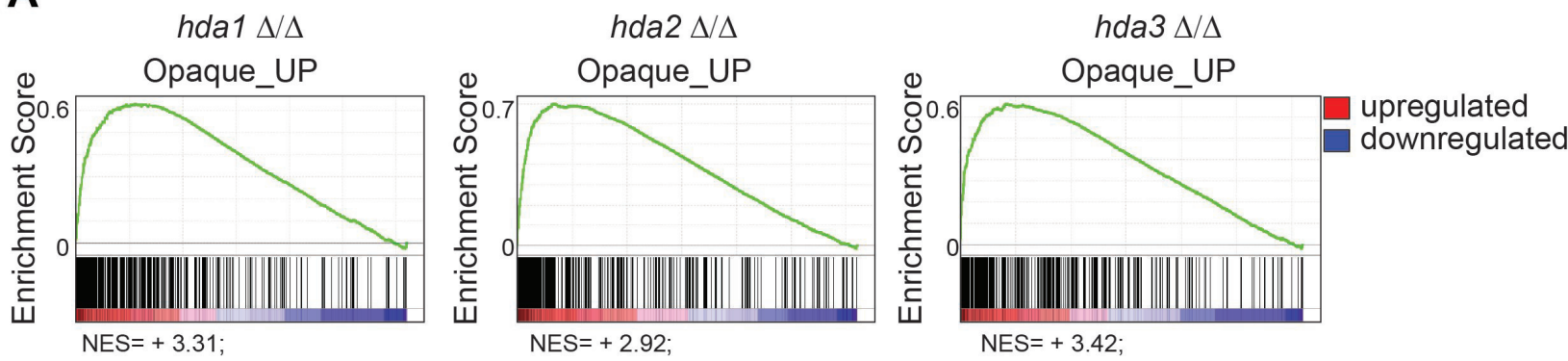
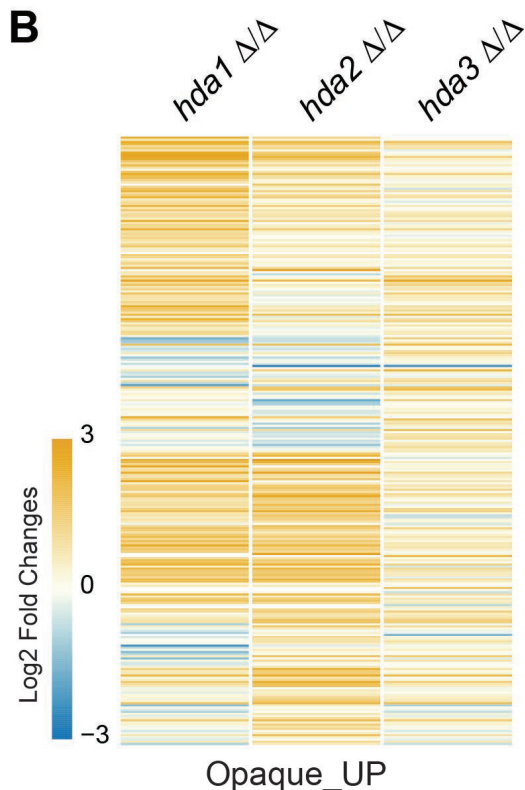
Response to Drugs



Host Interaction



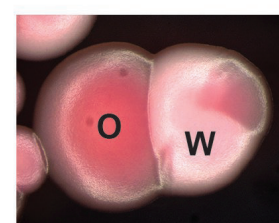
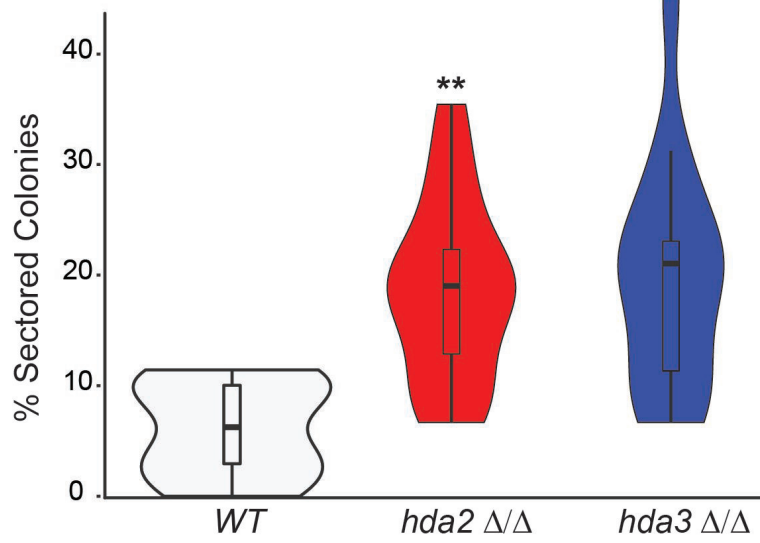
A**B**

A**B****C**

WOR1 (C1_10150W)

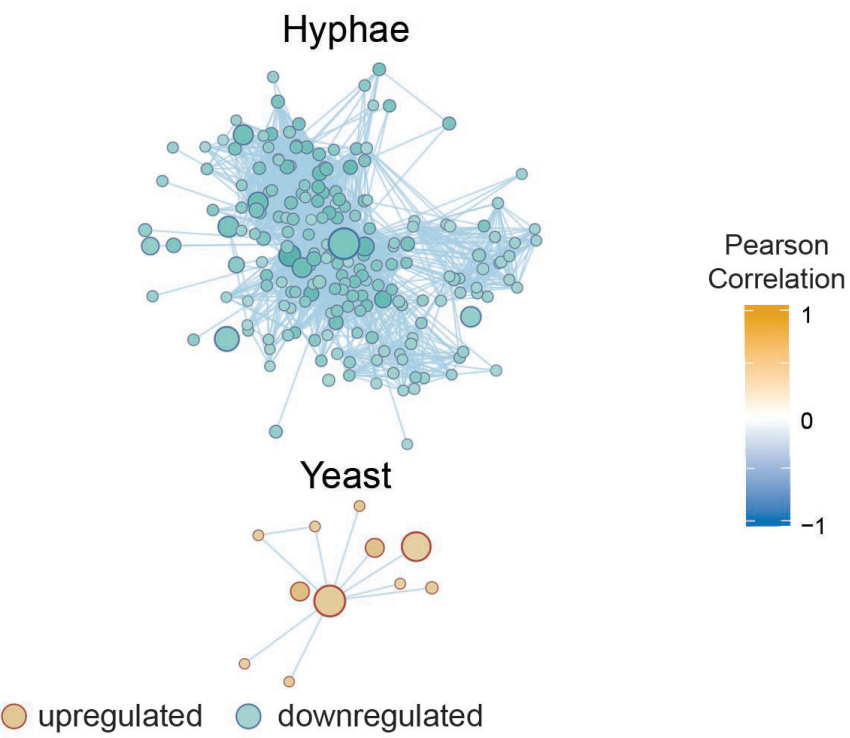
Strain	Log2 Fold change	p	q
<i>hda1</i> Δ/Δ	3.95	3.86 e-32	5.92 e-29
<i>hda2</i> Δ/Δ	2.46	4.61 e-13	2.67 e-10
<i>hda3</i> Δ/Δ	2.50	1.46 e-13	2.62 e-10

4
0
-4

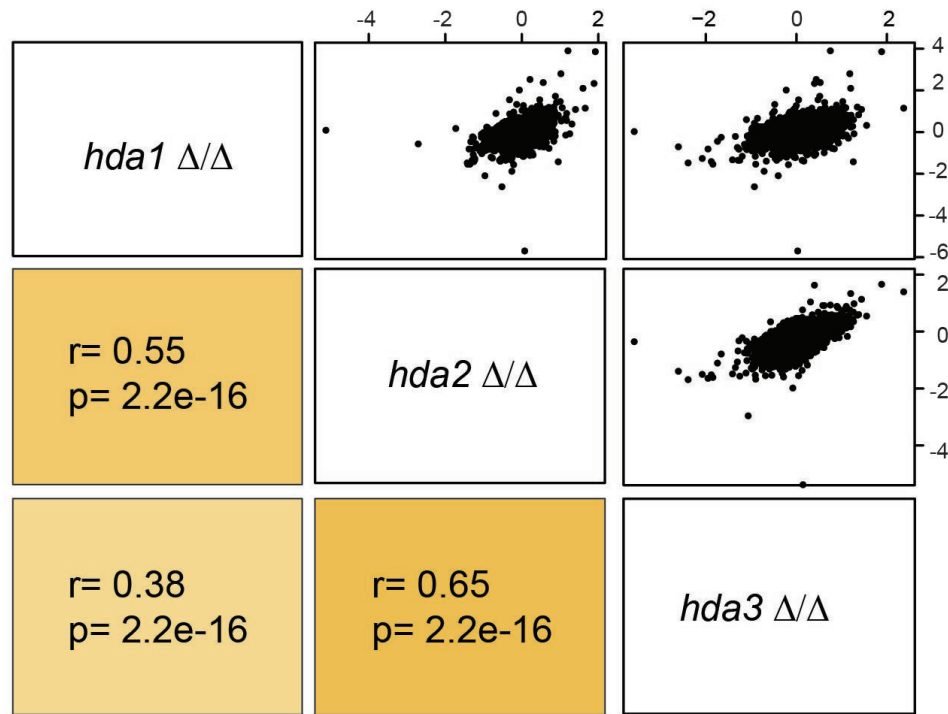
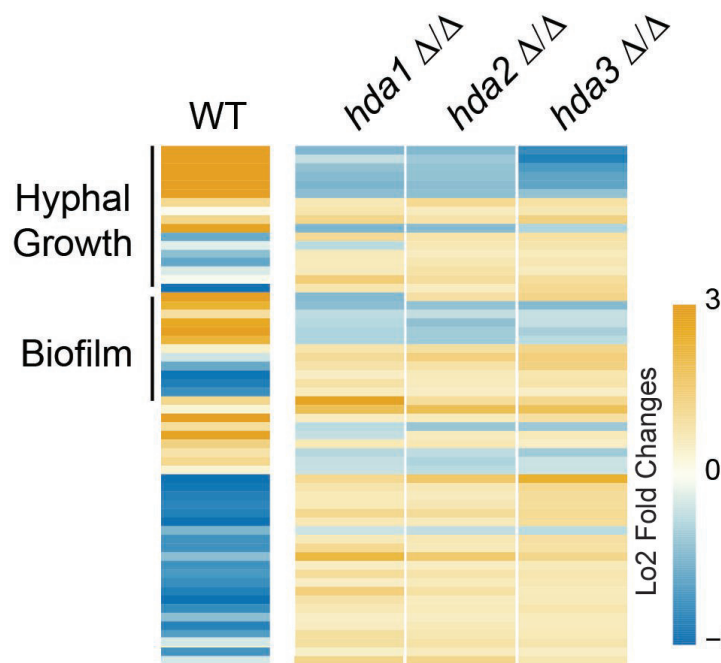
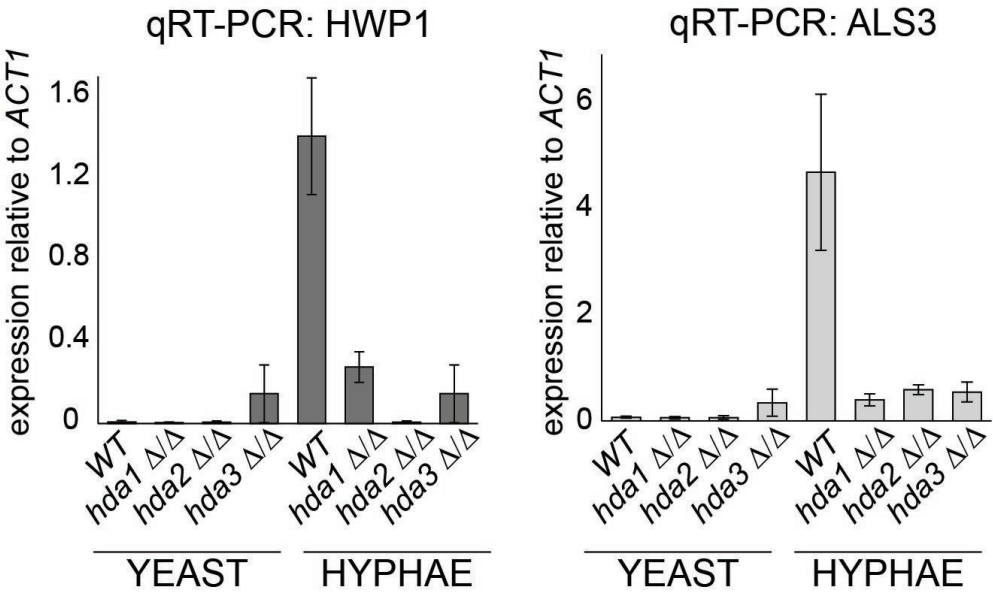
D

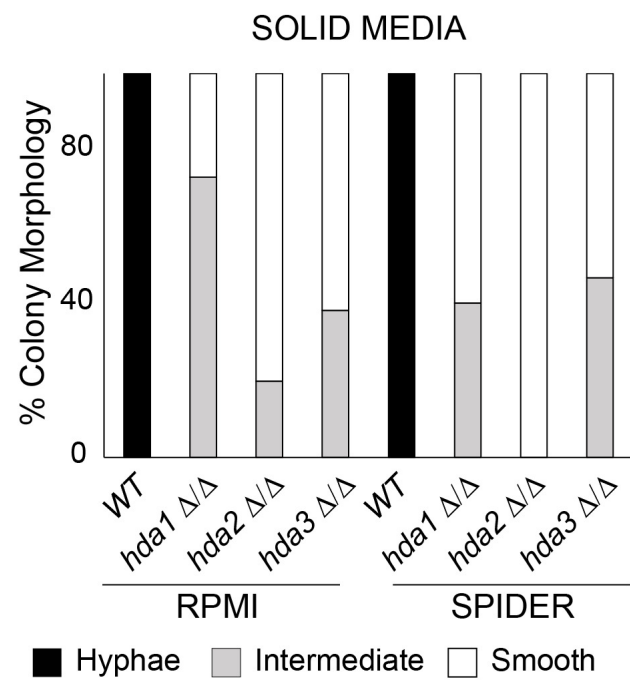
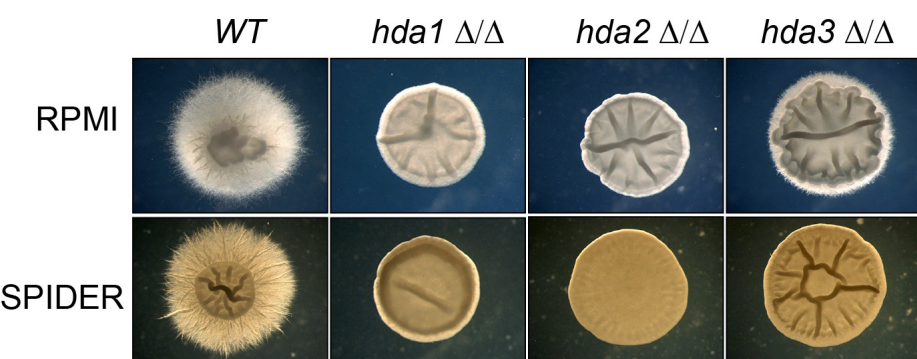
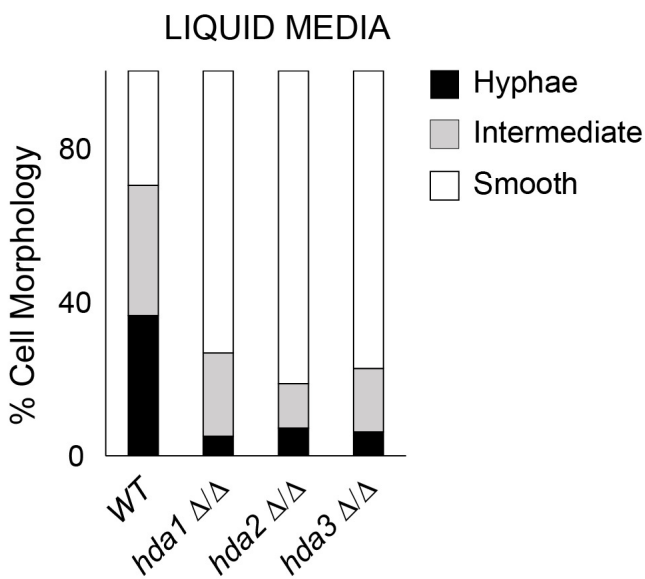
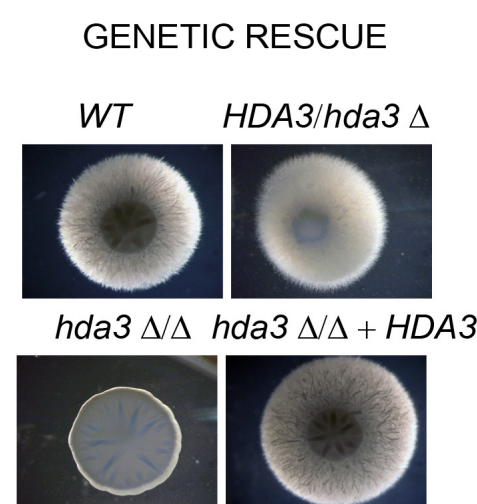
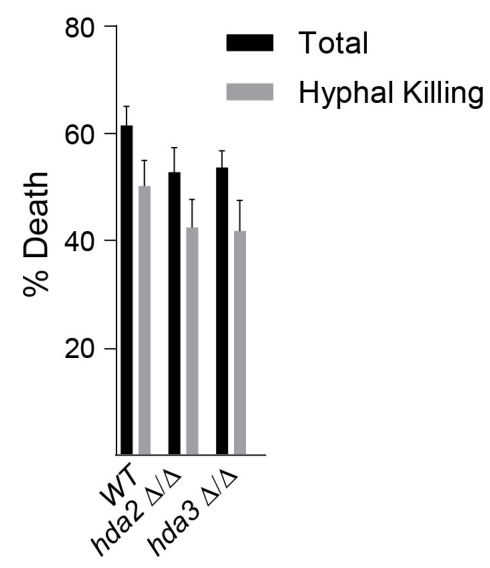
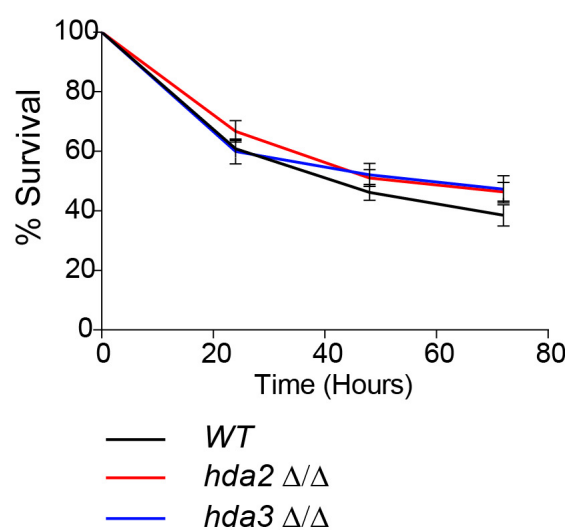
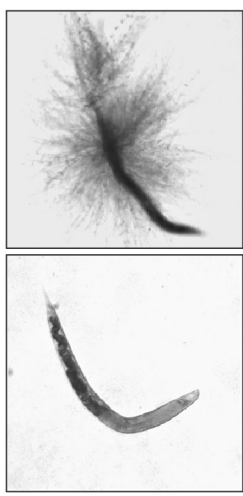
A

WT YPD vs RPMI

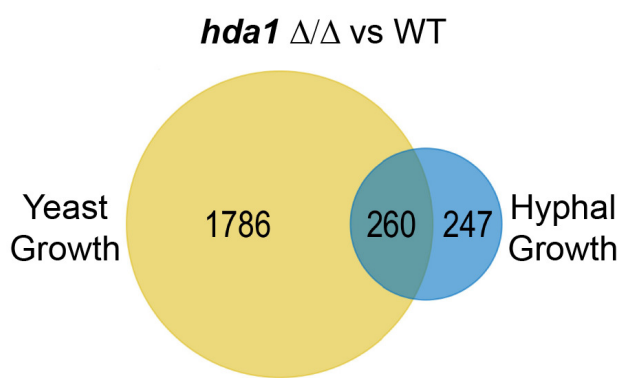
**B**

HYPHAE MEDIUM

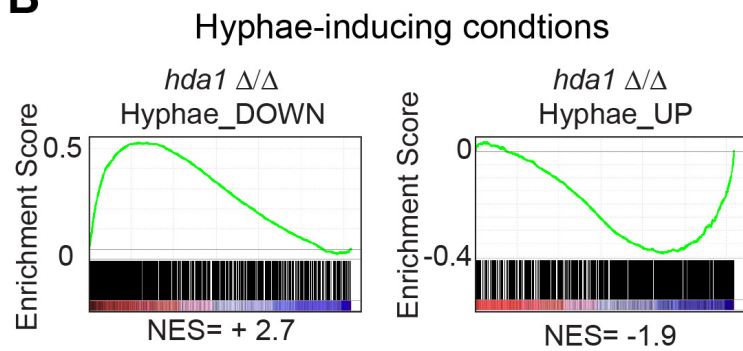
**C****D**

A**B****C****D**

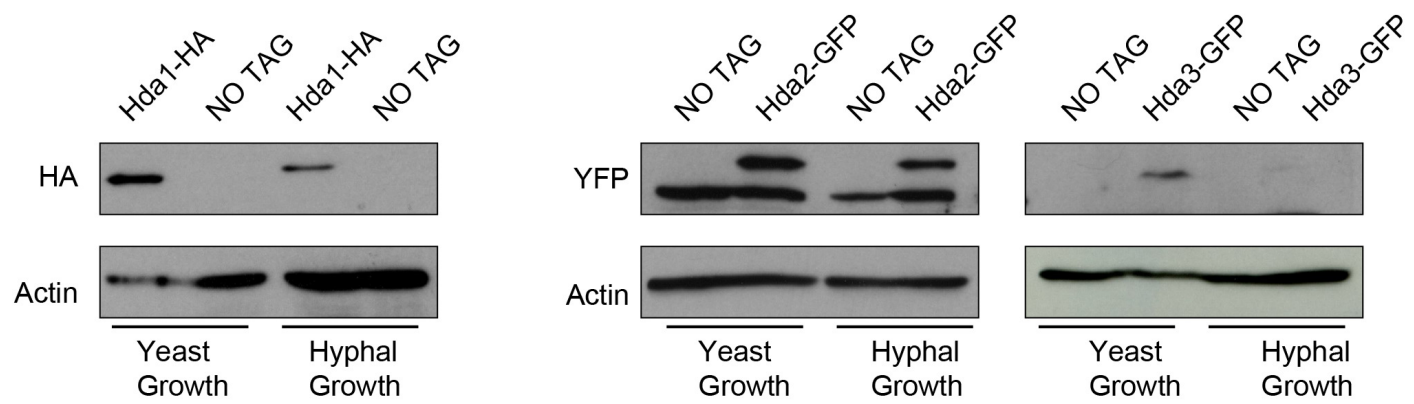
A



B



C



D

